



**HAL**  
open science

# A transmission electron microscopy study of experimentally deformed quartzite with different degrees of doping

David Mainprice, Olivier Jaoul

► **To cite this version:**

David Mainprice, Olivier Jaoul. A transmission electron microscopy study of experimentally deformed quartzite with different degrees of doping. *Physics of the Earth and Planetary Interiors*, 2008, 172 (1-2), pp.55. 10.1016/j.pepi.2008.07.009 . hal-00532162

**HAL Id: hal-00532162**

**<https://hal.science/hal-00532162>**

Submitted on 4 Nov 2010

**HAL** is a multi-disciplinary open access archive for the deposit and dissemination of scientific research documents, whether they are published or not. The documents may come from teaching and research institutions in France or abroad, or from public or private research centers.

L'archive ouverte pluridisciplinaire **HAL**, est destinée au dépôt et à la diffusion de documents scientifiques de niveau recherche, publiés ou non, émanant des établissements d'enseignement et de recherche français ou étrangers, des laboratoires publics ou privés.

## Accepted Manuscript

Title: A transmission electron microscopy study of experimentally deformed quartzite with different degrees of doping

Authors: David Mainprice, Olivier Jaoul

PII: S0031-9201(08)00176-3  
DOI: doi:10.1016/j.pepi.2008.07.009  
Reference: PEPI 5007

To appear in: *Physics of the Earth and Planetary Interiors*

Received date: 28-10-2007  
Revised date: 1-7-2008  
Accepted date: 11-7-2008

Please cite this article as: Mainprice, D., Jaoul, O., A transmission electron microscopy study of experimentally deformed quartzite with different degrees of doping, *Physics of the Earth and Planetary Interiors* (2007), doi:10.1016/j.pepi.2008.07.009

This is a PDF file of an unedited manuscript that has been accepted for publication. As a service to our customers we are providing this early version of the manuscript. The manuscript will undergo copyediting, typesetting, and review of the resulting proof before it is published in its final form. Please note that during the production process errors may be discovered which could affect the content, and all legal disclaimers that apply to the journal pertain.



A transmission electron microscopy study of experimentally deformed quartzite with different degrees of doping

David Mainprice<sup>1</sup>, Olivier Jaoul<sup>2</sup>

1 Université Montpellier 2, Géosciences Montpellier,  
CNRS/INSU, UMR 5243, CC 60,  
Place Eugène Bataillon, 34095 Montpellier, France

2 Université Paul-Sabatier, Laboratoire des Mécanismes et Transferts en Géologie,  
CNRS, Observatoire Midi-Pyrénées, 14 avenue Edouard Belin, 31400, Toulouse, France

\* corresponding author tel: +33-467143283; fax: +33-467143603  
e-mail: David.Mainprice@gm.univ-montp2.fr

Submitted to Physics of the Earth and Planetary Interiors  
Special Issue in honour of Olivier Jaoul

Submitted 27<sup>th</sup> October 2007

Revised version submitted 1<sup>st</sup> July 2008

A transmission electron microscopy study of experimentally deformed quartzite with different degrees of doping

David Mainprice<sup>1</sup>, Olivier Jaoul<sup>2</sup>

1 Université Montpellier 2, Géosciences Montpellier,  
CNRS/INSU, UMR 5243, CC 60,  
Place Eugène Bataillon, 34095 Montpellier, France

2 Université Paul-Sabatier, Laboratoire des Mécanismes et Transferts en Géologie,  
CNRS, Observatoire Midi-Pyrénées, 14 avenue Edouard Belin, 31400, Toulouse, France

\* corresponding author tel: +33-467143283; fax: +33-467143603  
e-mail: David.Mainprice@gm.univ-montp2.fr

---

## Abstract

TEM study of Heavitree quartzite deformed at high temperatures and a pressure of 1.5 GPa with three different preparations; water added, vacuum dried, and sodium doped show a wide range of dislocation microstructure. The vacuum dried sample has a very heterogeneous dislocation distribution varying from almost no dislocations to very high densities. Dislocation nucleation occurs by cross-slip mechanisms, such as Frank-Read sources and Orowan loops around hard inclusions. Shear bands develop in the basal plane composed of two closely spaced shear planes. Dislocations have straight segments and they are aligned along directions of dense packing, suggesting strong Peierls stress control due to the crystal structure. No voids, bubbles or dislocation walls were observed in the vacuum dried sample. The sodium-doped sample had a homogeneous high dislocation density. The water added sample has a significantly lower, relatively uniform dislocation density. Bubbles associated with dislocations are seen in every grain. Dislocations were either present in loops around bubbles or as straight dislocations with small bubbles spaced along the dislocation line. Some of the long straight dislocations are aligned parallel to the *c*-axis. Sub-grains were very frequent, sometimes form cells of about 2  $\mu\text{m}$  in diameter with straight edges. Analysis of dislocations show  $1/3\langle a \rangle$  and  $[c]$  dislocations in sub-grain walls and free  $1/3\langle a \rangle$  dislocations on prism planes. There is clear evidence for dislocation climb with sub-grain walls, dislocation cells, dislocation junctions and dislocation debris of small loops. The major difference between vacuum dried and water added samples is the homogeneity of the microstructure and evidence for climb in the water added sample. Glide is clearly difficult, with a high Peierls stress in the vacuum dried sample as shown by areas of very low and very high dislocation density and the crystallographic control of dislocation line direction. The sodium-doped sample indicates that nucleation was easy by the high homogeneous dislocation density, but no climb recovery has taken place. The density is high and the dislocations are strongly interacting causing tangles; no evidence for crystallographic control can be observed at these levels of strain.

The activation energy for creep in Heavitree quartzite decreases with inferred water content of the specimens from 185 kJ mole<sup>-1</sup> for vacuum dried to 151 for 0.4 wt% water added samples. Analysis of diffusion data for oxygen under hydrothermal conditions and inferred diffusion data for the hydrogarnet defect and dislocation velocity suggests activation energies for these processes are similar to the activation energy for the dislocation creep of Heavitree quartzite and other quartz aggregates. For data from the previously published experiments with the highest stress resolution there is a correlation between the A pre-factor in the power law creep equation and the activation energy for creep. It is speculated that the correlation may be due to variable hydrogarnet defect concentrations.

*Keywords:* Quartz; Hydrolytic weakening; Dislocation creep

---

## 1. Introduction

The plastic deformation of quartz is known to be strongly influenced by the presence of impurities at the parts per million (ppm) level, to the extent that pure defect-free quartz is not plastically deformable (see overview by Paterson, 1989; Blacic and Christie, 1984). It has long been established that presence of hydrogen related defects, often loosely called “water”, can reduce the plastic yield strength of quartz by an order of magnitude above some critical temperature at laboratory strain rates (Griggs and Blacic, 1965). It is often inferred that this hydrogen related defect should also be important in facilitating the plasticity of all silicates, as quartz contains structural elements common to many silicates. Despite the obvious importance of the “water” weakening mechanism, the details of how hydrogen related defects facilitate dislocation motion in quartz are still obscure after many years of study. The initial interpretation put forward by Griggs (Griggs and Blacic, 1965; Griggs, 1967) suggested that presence of water near the dislocation core reduced the energy necessary for a dislocation to glide by hydrolysing the strong Si-O-Si bond by the reaction:  $\text{Si-O-Si} + \text{H}_2\text{O} = \text{Si-OH}\cdot\text{HO-Si}$ , to produce the weak H•H bond. The weak hydrogen bond produced by this reaction causes the plastic weakening of quartz. The Griggs mechanism was strongly inspired by the hydrolysing reaction previously suggested for chemically assisted sub-critical crack growth in silicates glass by Charles and Hillig (1962). One implication of the Griggs mechanism is that the weakening defect has to be physically close to the dislocation core.

Many subsequent studies modified many of the initial conceptions about “water” weakening in quartz. With the application of transmission electron microscopy (TEM) to “water” weakened quartz a more complex vision was established with questions being asked about the role of “water” in the nucleation, multiplication, glide and climb of dislocations (e.g. McLaren et al., 1983, 1989). Efforts were made to clarify the mechanism of incorporation and solubility of water, revealing for example that; “water” in the original Griggs and Blacic experiments was introduced via microfractures not by diffusion into “dry” crystals (Kronenberg et al., 1986; Rovetta et al., 1986; Fitz Gerald et al., 1991) and the equilibrium solubility of “water” was in fact quite low at around 100 ppm (Kronenberg et al., 1986; Rovetta et al., 1986; Cordier and Doukhan, 1989). Inspired by the influence of charged defects on dislocations in semi-conductors (Hassen, 1979; Hirsch, 1979) and diffusion and creep rate of oxygen fugacity in olivine (e.g. Jaoul et al., 1981; Kolhstedt and Hornack, 1981) new theories about “water” weakening in quartz in terms of charged dislocation kinks by Hirsch (1981) and point defects by Hobbs (1981) opened the way to non-local thermodynamic models. It was in this new context that Jaoul et al. (1984) and Jaoul (1984) undertook a series of experiments on natural polycrystalline quartz (Heavitree quartzite, central Australia) with

different sample preparations. In this paper we will describe the dislocation microstructure of these deformed quartzites deformed in Griggs solid medium apparatus.

## 2. Sample Characterization and Preparation

The Heavitree quartzite is homogeneous with equant grains with a mean grain size of approximately 200 $\mu\text{m}$ . It is composed of quartz grains except for trace amounts of muscovite and iron oxide. The intrinsic major impurities (Al, Fe and K) in the quartz grains were measured using ion microprobe to have concentration levels of 60 Al/ $10^6$  Si, less than 40 for Fe/ $10^6$  Si and K/ $10^6$  Si. The infra-red spectrum of the 'as-received' or 'as-is' sample was studied at 78K by Mainprice (1981). The spectrum was analysed by using Gaussian components into three major subdivisions, 3 'gel' components at 2860, 3125 and 3475  $\text{cm}^{-1}$  that represent the broad absorptions, which do not change upon reducing the temperature from 298K to 78K, 1 muscovite component at 3630  $\text{cm}^{-1}$ , 1 structural OH at 3360  $\text{cm}^{-1}$  with a narrow half-width of 23  $\text{cm}^{-1}$  and 4 ice components at 3145, 3220, 3274 and 3380  $\text{cm}^{-1}$ . The 'gel' component contributes 2003 H/ $10^6$  Si and the ice (molecular water) contributes 756 H/ $10^6$  Si to a total "water" content of 2759 H/ $10^6$  Si of Heavitree quartzite using the Paterson (1982) IR calibration. This results compares favourably with the room temperature determination using a more modern Fourier transform infrared microscope by Kronenberg and Wolf (1990) of 3900 H/ $10^6$  Si. For reference 1000 H/ $10^6$  Si is equivalent to 0.015 wt% water in quartz.

Ideally we would like to use samples with controlled doping levels, however in this study the natural polycrystalline quartz was used as the starting material, variable "water" and sodium content was achieved by the methods described below; further descriptions can be found in Jaoul et al. (1984) and Jaoul (1984). To obtain the maximum of "water" concentration in the sample, which we will call "water-added", the natural sample was mechanically sealed with trace amounts of distilled water enriched in  $^{18}\text{O}$  in Pt jacket. After the deformation experiment the  $^{18}\text{O}$  was found to be uniformly distributed in the sample (Jaoul et al., 1984). Samples W-296 and W-300 are the "water added" samples with W-296 for 0.39Wt %  $\text{H}_2\text{O}$  (26 000 H/ $10^6$  Si) and 0.42 wt% (28 000 H/ $10^6$  Si) for W-300. As reported above the natural "as-received" or "as-received" sample already contains about between 4000 to 3000 H/ $10^6$  Si according to the infrared spectrum analysis and is reported by Jaoul et al. (1984) to contain 0.125 Wt %  $\text{H}_2\text{O}$  (8 300 H/ $10^6$  Si) based on weight loss during vacuum drying experiments. Clearly the "water" concentrations based on the Wt% values of Jaoul et al. could be a factor of 2 too high. The "dry" or low water content sample was prepared by vacuum drying the sample at 1010 $^\circ\text{C}$ , at vacuum pressure of 6 Pa, for 6 hours reducing the water content by 0.125 wt%. The sodium doping was done on samples that had been previously vacuum dried at high temperature and hence are "dry" samples in the sense of Jaoul et al. (1984). The diffusion of the sodium into sample W-301 was achieved by annealing the samples in liquid salt at 1113K for 15 minutes and the annealing at 973K for 5.5 hours (see Jaoul, 1984 for further details on individual samples). The equilibrium concentration predicted by the diffusion data of Rybach and Laves (1967) and Frischat (1970) should be 700 Na/ $10^6$  Si at 973K, close to the concentration 650 Na/ $10^6$  Si for sample W-301, measured by bulk chemical analysis using direct current argon plasma atomic emission spectroscopy. However, electron microprobe analysis with 2  $\mu\text{m}$  diameter beam showed the concentration was only 350 Na/ $10^6$  Si in the grain interiors and 3000 Na/ $10^6$  Si at the grain boundaries. The diffusion conditions were such that both samples W-301 and W-303 contain the same concentration, which are about a factor 2 smaller than equilibrium values quoted by Rybach and Laves (1967). Note that concentration of sodium at 350 Na/ $10^6$  Si is significantly higher than 60 Al/ $10^6$  Si or 40 for Fe/ $10^6$  Si of the vacuum dried sample. Hence in the following we

consider W-296 and W-300 (“water-added”) to be high “water” content samples, W-284 (“as-received”) to be moderate “water” content, W-301 and W-303 sodium-doped samples and W-302 (“vacuum dried”) to be aluminium doped or nearly pure. It should be noted that a recent set of experiments by Stipp et al. (2006) using Black Hills quartzite and a slightly different protocol for the “water-added”, “as-received” and “vacuum dried” sample preparation, report that “water” content measured after the deformation experiment is highest for “water-added” and lowest for “vacuum dried”, with “as-received” having an intermediate content for Black Hills quartzite. However, all the post-mortem water contents are lower than the initial concentration of the as-received Blackhills quartzite of about  $2600 \text{ H}/10^6 \text{ Si}$  (average of 3 samples). We consider that “water-added”, “as-received” and “vacuum dried” sample preparation can depend on a number of experimental details and can only give a relative scale of “water” concentration that is consistent within a study.

### 3. Experimental procedures and results

The majority of experiments of reported by Jaoul et al. (1984) and Jaoul (1984) were creep experiments done in Griggs deformation apparatus at 1.5 GPa pressure, using NaCl at lower temperatures and  $\text{CaCO}_3$  above  $900^\circ\text{C}$  as the pressure medium. Samples of 6 mm diameter and 12 mm length were mechanically sealed in a Pt tube with Pt caps. The Pt tube was placed inside a thin (0.1 mm) Ni tube. One set of creep tests was done at constant temperature with a number of different stresses to determine the stress exponent of power law creep. A second series of creep tests was done at constant differential stress and number of different temperatures to determine the activation energy. Samples from runs W-300, W-303 and W-302 where selected for TEM observations (see Table 1). Run W-300 (water added) was a constant strain rate test at  $900^\circ\text{C}$ . Run W-303 (Na-doped) was a creep test at temperatures of 800 and  $890^\circ\text{C}$ . Run W-302 (vacuum dried) was a creep test at constant temperature of  $890^\circ\text{C}$ . The samples for TEM were prepared by standard ion thinning techniques to electron transparency. TEM observations where made on JEOL 120kV microscopy at the University of Nantes (France) and a 1000 kV instrument at the University of Oxford (England).

The mechanical properties are illustrated in figure 1 for a temperature of  $800^\circ\text{C}$  at a pressure of 1.5 GPa. As expected the “water added” sample is the weakest and significantly weaker than the “as-received” sample. The sodium-doped samples are stronger than the “as-received” sample, but significantly weaker than the “vacuum dried”. For a differential stress of 0.5 GPa the strain rates of the “water added”, “as-received”, sodium-doped and vacuum dried samples are  $1 \times 10^{-5}$ ,  $3 \times 10^{-6}$ ,  $3 \times 10^{-7}$  and  $3 \times 10^{-8} \text{ s}^{-1}$  respectively. If we use the vacuum dried sample as our reference strain rate, then sodium doping increases the strain rate by order of magnitude, where as the presence of water increases the strain rate by two to nearly three orders of magnitude depending on the concentration.

### 4. Microstructure

In order to understand these order-of-magnitude changes in strain rate at laboratory conditions the microstructure of samples W-300, W-303 and W-302 were studied using conventional TEM techniques using bright and dark field imaging. The majority of imaging was done in bright field. Dislocations where characterised by tilting experiments to determine the dislocation line and using the dislocation ‘invisibility’ criteria to identify cases where the diffracting vector  $\mathbf{g}$  is perpendicular to the Burger’s vector  $\mathbf{b}$  ( $\mathbf{g}\cdot\mathbf{b}=0$ ). The symmetry and stability of the dislocation image with deviation from the exact Bragg condition was also used to identify  $\mathbf{g}\cdot\mathbf{b}=0$ . We initially assumed that dislocations with Burgers vectors  $\mathbf{b}=1/3\langle\mathbf{c}+\mathbf{a}\rangle$  to

be unlikely to simplify our analysis, but in fact there was rarely ambiguity caused by the potential presence of  $1/3\langle\mathbf{c}+\mathbf{a}\rangle$  dislocations.

Sample W-300 is the water-added sample with 0.42Wt%  $\text{H}_2\text{O}$ . Traces amounts of amorphous  $\text{SiO}_2$  were seen on grain boundaries of this sample (Figure 2 a, b, c). The amorphous material shows a clear ring diffraction pattern and is fractured indicating that materials formed at high pressure and temperature during the deformation experiment and fractured by differential contraction on cooling. The amorphous material is almost certainly a melt film that formed at triple junctions, which reacted with the quartz to form curved pockets at triple junctions. Some localized dislocation activity was observed near contacts between rounded grains (figure 2c). Other grain boundaries appeared to be melt-free with strong Moiré fringes indicating low angle crystallographic mismatch (figure 2d). Some grain boundaries appear to be stepped (Figure 2d, Figure 2a and b) or pinned by voids. Low angle sub-grain boundaries are frequent, often displaying variable crystallographic orientation consistent with variable local dislocation density in the sub-boundary and surrounding regions (figure 3c). Dislocations are often linked to voids in these regions (Figure 3). Sub-grains form cell-like structures with straight edges as can be seen in Figure 4a with a diameter of approximately  $2\mu\text{m}$ . Analysis of the sub-grain wall in 4b,c,d under different diffracting conditions reveals that  $\mathbf{b}=1/3\langle\mathbf{a}_1\rangle$  dislocations are out of contrast for diffraction vector  $\mathbf{g}=(0\ 1\ \bar{1}\ \bar{1})$  in figure 4b and 4c, whereas  $[\mathbf{c}]$  are out of contrast for  $\mathbf{g}=(0\ 1\ \bar{1}\ 0)$  in figure 4d. The sub-grain wall is close to the  $(2\ \bar{1}\ \bar{1}\ 0)$  plane, which is normal to the beam direction. The geometry of the  $1/3\langle\mathbf{a}_1\rangle$  dislocations line direction is  $\mathbf{u}=[0\ 1\ \bar{1}\ 0]$  consistent with a pure edge ( $\mathbf{b}$  to  $\mathbf{u}=90^\circ$ ) dislocation gliding in (0001) plane. The  $\mathbf{b}=[\mathbf{c}]$  with the dislocation line direction  $15^\circ$  from [0001] in the sub-grain wall, consistent with a near screw dislocation gliding in the  $(2\ \bar{1}\ \bar{1}\ 0)$  plane. Further dislocation analysis of isolated dislocations using four different diffracting vectors  $\mathbf{g}_1=(\bar{1}\ 0\ 1\ 1)$ ,  $\mathbf{g}_2=(1\ \bar{2}\ 1\ 2)$ ,  $\mathbf{g}_3=(2\ \bar{2}\ 0\ 1)$  and  $\mathbf{g}_4=(1\ 0\ \bar{1}\ 2)$  show progressively increasing radiation damage during the course of the tilting experiment (Figure 5). The first image (figure 5a) shows dotted black-white contrast, which did not change on increasing deviation from the Bragg exact condition ( $W=0$ ). Stable dotted black-white contrast with increasing deviation from the Bragg condition ( $W>0$ ) is a characteristic of  $\mathbf{g}\cdot\mathbf{b}=0$  for dislocations inclined to specimen surface in anisotropic elastic crystals (e.g. Mainprice, 1981; Montardi and Mainprice, 1986). Stable images with  $W>0$  are observed for  $\mathbf{g}_1$  and  $\mathbf{g}_4$  (figure 5a,d), despite the fact that radiation damage is clearly visible in the background of figure 5d. From the geometry determined from the tilting experiment the dislocations have a line direction  $\mathbf{u}=[1\ \bar{2}\ 1\ 2]$  consistent with  $\mathbf{b}=1/3\langle-\mathbf{a}_2\rangle$  mixed ( $\mathbf{b}$  to  $\mathbf{u}=36.25^\circ$ ) dislocation gliding on (10-10) plane.

The vacuum dried sample W-302 has a totally different microstructure with a very heterogeneous dislocation density. The extreme variation in dislocation density is well illustrated by figure 6a taken using a high voltage (1000 kV) TEM, where regions of several  $\mu\text{m}^2$  that have absolutely no dislocations are adjacent to shear bands in the (0001) plane. The shear bands appear to be in the basal plane, but they are not perfectly straight. The shear bands have structure composed on two planes of high-density dislocations separated by about  $0.25\ \mu\text{m}$ . In the  $0.25\ \mu\text{m}$  interval the dislocation contrast is attenuated. The dislocations are nucleated above and below the twin shear planes that are perpendicular to the (0001) plane (Fig.6a); given the beam direction is  $[1\ 3\ \bar{2}\ \bar{1}\ 2]$  and the diffracting vector  $\mathbf{g}=(1\ \bar{3}\ 2\ 1)$ , the low index plane perpendicular to the (0001) is  $(1\ 0\ \bar{1}\ 0)$  for this field of view. The

dislocations emanating from the (0001) shear band and gliding on the  $(1\ 0\ \bar{1}\ 0)$  plane show clear evidence for structural control of their line direction. At the top of figure 6a the dislocations form loops with straight segments with an intersection angle of  $103^\circ$ , consistent with the intersection of the densely packed rhombohedral planes  $\{1\ 0\ \bar{1}\ 1\}$ . On the lower side of the shear band the dislocations loops have three linear segments; their intersection at  $128^\circ$  is controlled by the segments changing from positive rhombohedral planes (**r**) to the basal plane (**c**) to the negative rhombohedral plane (**z**). Nucleation of these loops involves a Frank-Read source (marked FR in the figure and enlarged in inset figure), which allows the formation of closely spaced slip bands. Frank-Read sources are created by the multiple cross-slip of a screw dislocation onto an adjacent parallel slip plane to form two immobile segments. As the two immobile edge segments originated from a single screw dislocation, a line joining the two edge immobile segments should be parallel to the Burger's vector of the original screw dislocation; in Figure 7a, this must be **[c]** as the line is normal to (0001) plane of the shear bands. The minimum applied stress to operate a Frank-Read source can be estimated from  $\sigma = 2Gb/L$ , where *G* is the shear modulus (44.3 GPa for  $\alpha$ -quartz), **b** the Burgers vector (5.4 Å for **[c]**), and the separation of two immobile edge segments is about 0.1  $\mu\text{m}$  (fig. 6a), giving a stress 0.4 GPa, well below the 0.5 to 1.0 GPa differential stresses applied to this sample (Figure 1). Regions of high-density dislocations and (0001) shear bands are seen in Figure 6b with diffracting vector  $\mathbf{g} = (0\ \bar{1}\ 1\ 0)$ ; with this vector **[c]** dislocations should be invisible or show weak contrast. Indeed no such dislocations are seen in this image. The dislocations with straight-line segments controlled by the crystal structure are  $\langle a \rangle$ . In figure 6c two very high dislocation density (0001) shear bands are present, but the bands have almost no contrast with a high structure factor diffracting vector  $\mathbf{g} = (\bar{1}\ 0\ 1\ 1)$ , where as the adjacent areas have high contrast and relatively low dislocation density. There is almost certainly some misorientation between the shear bands and the matrix that could explain some of the contrast attenuation, but the presence of high density of  $1/3\langle a_2 \rangle$  dislocations, which should out of contrast with  $\mathbf{g} = (\bar{1}\ 0\ 1\ 1)$ , could also explain the contrast variations.

One of the key factors for explaining the variation of mechanical properties between samples is the mechanism of dislocation nucleation (cf McLaren et al., 1989). In the water-added specimen (W-300) the presence of voids associated with dislocations is very frequent (Figure 7a,b). The dislocations form loops around voids (Figure 7a) or the voids are along the dislocation lines (Figure 7b). In many cases the dislocation loops and lines are parallel to the **[c]** direction (Figure 7a,b). The voids may be filled with water (bubbles), but we cannot confirm this with our TEM observations. The voids, loops and dislocations lines in the water-added sample are homogeneously distributed. Note there is no manifestation of strain field associated with the voids. In contrast the vacuum dried sample (W-302) very heterogeneous dislocation densities are always present (Figure 6). The nucleation mechanism appears to be by dislocation multiple cross-slip (e.g. Frank-Read source, Figure 6a), and the very high densities will also result in significant nucleation by the dislocation-dislocation interaction. We have also observed dislocation nucleation at small solid precipitates (Figure 7c), where multiple small and large loops are generated. The geometry of the dislocation loops is exactly as described by Hirsch and Humphreys (1970) for small impenetrable particles. When a critical number of Orowan loops are exceeded there is interference between stress fields of gliding dislocations and the loops generated at the particle. The interaction between the gliding dislocation and Orowan loops around the hard particle results in a cross-slip process for the generation of prismatic vacancy loops. It is evident from Figure 7c that this mechanism is extremely efficient at generating dislocations, however composition and origin

of precipitates is unknown, and hence general significance of this observation is difficult to access. Note however that this dislocation source is also a cross-slip mechanism like the Frank-Read source that does not require climb. The sodium-doped specimen (W-303) was very difficult to observe in TEM because of very high uniform dislocation density, which made it impossible to observe individual dislocations. Figure 7d is a typical observation near a grain boundary, with an isolated dislocation (marked d) on the grain boundary showing oscillating contrast with depth in the specimen. The contrast is almost uniform black due to the very high dislocation density.

## 5. Discussion

The TEM observations presented here when combined with mechanical data of Jaoul et al. (1984) and Jaoul (1984) provide the basis for discussing the deformation mechanisms in the context of the various theories on the effects of doping on quartz. We will not develop details of these theories here, but refer the reader to the original papers. From the mechanical data we have seen the different sample preparations leading to strain rates from  $3 \times 10^{-8} \text{ s}^{-1}$  for vacuum dried sample to  $1 \times 10^{-5}$  for the water added sample at differential stress of 0.5 GPa, 800°C and confining pressure 1.5 GPa. From the TEM observations we have seen that dislocations are present at moderate to high densities in all samples, so that we should consider a dislocation mechanism to be rate controlling. The presence of significant dislocation climb, for example as shown by sub-grain walls (figure 3c,4b), dislocation cells (figure 4a) and dislocation junctions (figure 3c,4b) is only found in the water-added sample. Both  $\langle a \rangle$  and  $[c]$  Burgers vectors were observed. The  $\langle a \rangle$  appear to be more common, especially in the vacuum dried sample, but both appear to be necessary for strain compatibility in polycrystalline samples. The exact concentration of “water” and sodium is rather poorly defined, especially for “water” because no post-mortem analysis was undertaken. Post and Tullis (1998) reported that samples of Heavitree quartzite vacuum dried at 800°C at 6 Pa for 12 hours contained  $240 \text{ H}/10^6 \text{ Si}$ , where as our samples were dried at 1010°C, 6 Pa for 6 hours. More recent work by Stipp et al. (2006) suggests only relative “water” concentration values can be applied to vacuum dried, as-received and water added samples. TEM observations reveal the extensive presence of voids (or bubbles) in the water-added sample, where as none were observed in vacuum dried samples. Voids are also intimately associated with straight dislocations parallel to the c-axis (e.g. fig. 7b). Other long straight dislocations parallel to c-axis were seen in regions of low dislocation density (figure 3d), a direction which has relative fast oxygen diffusion (Dennis, 1984; Giletti and Yund, 1984). Field ion microscopy has shown that voids tend to nucleate at point defects or clusters of point defects, in quenched or irradiated materials (Baluffi and Seidman, 1972). Nucleation in the vacuum dried sample occurs by mechanisms involving cross-slip (e.g. Frank-Read source), confirming that climb is not very active in this sample. The presence of melt pockets in the “water added” sample at some grain boundary triple junctions certainly complicates the “water” budget as up to 10 wt% water can be dissolved in a  $\text{SiO}_2$  melt phase (Wu 1980; Mainprice, 1981; Mainprice and Paterson, 1984), however the melt fraction is very small, probably less than 1%. Mechanically the presence of melt may have had some effect as the stress exponent of the power law varies from 1.8 for water added, to 2.3 for as-received to 3.3 for sodium doped and vacuum dried. The samples with little or no water, and hence no melt have a slightly higher stress exponent 3.3 (see Table 1). Additional information that may be useful for comparing with theory is the activation energy for creep given in Table 1. In figure 8 we have plotted the activation energy as a function of water content, although we emphasize that the water content is only qualitative, the plot shows that the trend is towards lower activation energy at higher water content.

In considering the problem of hydrolytic weakening and the effects of doping in the dislocation creep regime, one should first consider the equation for strain rate associated with expansion of a dislocation loop, sometimes called Orowan's equation,

$$\dot{\epsilon} = \alpha b \rho_m \bar{v}$$

where the strain rate ( $\dot{\epsilon}$ ) is equal to a geometrical factor to account for the orientation of the dislocation slip system with respect to the applied stress ( $\alpha$ ), the Burgers vector ( $b$ ), the mobile dislocation ( $\rho_m$ ) and average dislocation velocity ( $\bar{v}$ ) of a loop in the direction of the normal to the dislocation line. One can see immediately that the variables mobile dislocation density and dislocation velocity are the key parameters in controlling the plastic strain rate for a given geometrical orientation. The mobile dislocation density is some fraction of the total dislocation density controlled initially by the presence of some mechanism to generate dislocations. The presence of any imperfection in a crystal can be the source of stress amplification that leads to dislocation nucleation. In the case of hydrolytic weakening, precipitates (e.g. Morrison-Smith et al., 1976) and bubbles (e.g. McLaren et al., 1983, 1989) have been proposed as major sites of dislocation nucleation in synthetic crystals. Almost all observations of naturally deformed quartz also mention the presence of bubbles. In general nucleation does not appear to be difficult in quartz except in dry (and pure?) crystals, which appear to be the rare. The vacuum dried sample appears to be at this end of the spectrum with nucleation being extremely localized with areas of no dislocations (Figure 6). In the water-added and sodium doped samples, dislocation nucleation is not a problem as moderate to high uniform density of dislocations are present in both samples. Hence, we conclude that when weakening occurs that dislocation nucleation is not the rate-limiting step. Even in the vacuum dried sample there are areas of more uniform dislocation density (Figure 6b); however, this may be due to the heterogeneous nature of the dehydration process as Post and Tullis (1998) report that some "water" remains in vacuum dried samples.

We will now focus our attention on the average mobile dislocation velocity; this is likely in our opinion to be the rate-controlling step. In the case of conservative glide (i.e. no climb occurs), it is known in many materials, for example LiF (Johnston and Gilman, 1959), that dislocation velocity can vary over 12 orders of magnitude when the applied shear stress is increased by 3 orders of magnitude. The dislocation velocity varies with stress to a power  $m$ , where  $m$  is typically in the range 1 to 5. Hence variations in the dislocation velocity could easily explain the 3 orders of magnitude increase in strain rate from vacuum dried to water added samples. Kirby and McCormick (1979) have presented a velocity law for wet synthetic quartz as

$$v = v_0 \exp(-Q/RT)(\tau/\tau_0)^m$$

where  $v_0$ ,  $Q$ ,  $\tau_0$ ,  $m$  are constants, with the stress exponent  $m=2.5 \pm 0.4$  and activation energy  $Q=163 \pm 21$  kJ/mole. Is the dislocation velocity controlled by interaction with obstacles (e.g. dislocations in other slip planes, voids, bubbles or precipitates), its intrinsic glide rate in the slip plane, climb rate, some other chemical process or is it controlled by some combination of these processes? Kirby and McCormick (1979) have examined the problem of obstacles in some detail, where their water-rich (out of equilibrium) synthetic crystals were continuously precipitating water at room pressure, and they have concluded that obstacle related hardening was not the major factor in the observed decrease in strain rate in their experiments. They also noted that  $v_0$  increased with the initial water of their crystals, where as the parameters  $m$  and  $Q$  did not show any systematic variation. The glide rate is well known to vary with doping concentration in semi-conductors, and this fact encouraged Hirsch (1981) to propose a conceptual model for hydrolytic weakening of quartz based on an electronic doping effect that should result in a non-local effect of overcoming high Peierls energy barriers caused by the atomic crystal structure. We have chosen silicon as the example that is chemically the closest

to quartz. The introduction of an electrically active impurity, which donates free electrons to the conduction band (n-type dopant, e.g. As, Sb, P) or accepts electrons from the valence band (p-type e.g. B, Al) at concentration levels of  $10^{19}$  to  $10^{20}$   $\text{cm}^{-3}$  increases the dislocation velocity in silicon relative to the pure material by approximately an order of magnitude (Patel et al. 1976; Yonenaga, 2001). The effect of the p-type acceptor dopant is comparatively weak, however the velocity increases monotonically with concentration of both p- and n-type dopants in silicon. The pre-exponential factor ( $v_0$ ) also decreases from  $10^7$  to  $10^4$   $\text{cm s}^{-1}$  with increasing concentrations of p- and n-type dopants. Note that impurities that are electrically neutral (i.e. same charge as Si, e.g. Ge) will only interact with dislocations via the elastic strain fields they produce, causing for example pinning, which may result in a threshold stress to activate glide. The experimental results of Patel et al. (1976) have been interpreted in terms of concentrations of charged kinks by Schroter et al. (1977) and Hirsch (1977). The general idea is that dislocations lie in the Peierls energy valleys and under the action of applied stress the dislocations move to the next valley by nucleating kink pairs, which migrate by expanding sideways. Fundamental quantities are the kink concentration (or nucleation rate) and the kink migration velocity. The concentration levels ( $10^{-18}$   $\text{cm}^{-3}$ ), which are high for semi-conductor applications, are the same order of magnitude as the  $100 \text{ H}/10^6 \text{ Si}$  commonly considered critical for hydrolytic weakening (e.g. Paterson 1989; Cordier and Doukhan, 1989). Within experimental scatter the activation energy for glide in silicon is  $220 \text{ kJ mole}^{-1}$  ( $2.25 \text{ eV}$ ) and the power-law stress dependence has an exponent  $m \approx 1$  for pure crystals for stresses between 3 to 30 MPa (Yonenaga, 2001). The charged dislocation kink theory can account for the experimentally established variation in activation energy with doping (Figure 9) in silicon, decreasing the activation energy by  $-78 \text{ kJ mole}^{-1}$  ( $-0.8 \text{ eV}$ ) for n-type and  $-49 \text{ kJ mole}^{-1}$  ( $-0.5 \text{ eV}$ ) for p-type. We can conclude from the experimental data on silicon that the dislocation velocity can be increased by order of magnitude in the temperature range  $600\text{-}950^\circ\text{C}$  and that the activation energy can change by 80 to 50  $\text{kJ mole}^{-1}$  (36-22% decrease) and the pre-exponential factor ( $v_0$ ) decreases by three orders of magnitude with increasing electrically active impurity concentration. Apart from the deductions by Kirby and McCormick (1979) from their creep experiments, no direct measurements have been made on the dislocation velocity in quartz.

Dislocation climb is an important mechanism, which allows dislocations to move out of their glide plane and avoid obstacles. In general, dislocation climb is not usually considered as a mechanism that introduces significant plastic strain (cf Nabarro-Herring creep), but it allows dislocations to continue to glide. For a dislocation to climb in quartz, vacancies (or interstitials) of both oxygen and silicon are necessary for the dislocation line to move up and out of the glide plane, which is more likely to occur at high temperature where the concentrations are highest. Climb is considered by many to be the rate controlling step in quartz deformation (e.g. Gleason and Tullis, 1995; Post and Tullis, 1998). Diffusivity depends on the concentration and mobility of the diffusing defect (e.g. vacancies or interstitials). In this sense it is formally similar to the situation for dislocation glide given by Orowan's equation; thus electronic defect models have been proposed as a universal explanation of diffusion, glide and climb processes in semi-conductors and insulators (e.g. Hobbs, 1981, 1984; Hirsch, 1981). In a similar way to kinks on a gliding dislocation, the climb of a dislocation can be formulated in terms of charged jogs. Essential to the understanding of quartz deformation involving dislocation climb is knowledge of the diffusivity of silicon and oxygen point defects. The first determination of silicon diffusion along the c-axis by Giletti et al. (1976) was published as an abstract reported  $D_0 = 2.0 \times 10^{-10} \text{ m}^2 \text{ s}^{-1}$ , activation energy of  $230 \text{ kJ mole}^{-1}$ . Jaoul et al. (1995) measured the diffusivity of silicon in a very pure synthetic crystal along the c-axis, which showed that diffusivity was very slow at  $10^{-20}$  to  $10^{-17} \text{ m}^2 \text{ s}^{-2}$  between  $1400$  and  $1600^\circ\text{C}$  with a pre-exponential factor  $D_0 = 1.3 \times 10^{-10} \text{ m}^2 \text{ s}^{-1}$ , an activation

energy of  $745 \text{ kJ mole}^{-1}$  (7.6 eV). No effect of pressure was observed between  $10^{-4}$  to 2 GPa. The diffusivity and activation energy are similar to corresponding values for vitreous silica. Jaoul et al. (1995) suggested that the diffusion mechanism could not be a silicon vacancy mechanism due to relatively low activation energy and similarity with vitreous silica. The authors argued for an interstitial mechanism involving a Frenkel pair consisting of a silicon vacancy and an interstitial silicon which should be insensitive to oxygen partial pressure. Clearly this diffusive mechanism could not be operative during hydrolytic weakening of defect rich crystals and it is unfortunate we do not have a complete study of Si diffusion under hydrothermal conditions. Oxygen diffusion in quartz has been measured by several authors, (see Brady, 1995 for a compendium). Hydrothermal studies in unbuffered conditions by Dennis (1984) and Giletti and Yund (1984) at 100 MPa in the  $\beta$ -quartz field both showed that diffusion of oxygen was three orders of magnitude faster along the c-axis than in the basal plane. The activation energies for diffusion along the c-axis were  $138.5$  and  $142.0 \text{ kJ mole}^{-1}$  respectively for Dennis (1984) and Giletti and Yund (1984), where as for diffusion in the basal plane they were  $203.7$  and  $234.0 \text{ kJ mole}^{-1}$ . More recently Farver and Yund (1991) determined the activation energy to be  $243 \text{ kJ mole}^{-1}$  for  $\alpha$ -quartz parallel to the c-axis at  $450$ - $590^\circ\text{C}$  and 100 MPa confining pressure. Farver and Yund (1991) show that in their buffered experiments, there was a good correlation with water fugacity, but no correlation with either oxygen or hydrogen fugacities, or with proton activity. They suggested that the oxygen-bearing species responsible for the rapid transport of oxygen under hydrothermal conditions is molecular water. The rate-controlling step for oxygen diffusion may be either the rate of migration of water molecules, or the rate of oxygen exchange between the water molecules and the quartz structure. McConnell (1995) suggested that solubility of water molecules in the c-axis channel was only  $10^{-4}/10^6 \text{ Si}$  at  $500^\circ\text{C}$  and 200 MPa based on ab initio calculations, and the concentration of molecular water within the c-axis channel of quartz is linearly dependent on the fugacity of the external water, in agreement with Farver and Yund (1991) experiments. McConnell's calculations also support the idea that the rate-controlling step for oxygen diffusion is the self-diffusion coefficient of interstitial water within the quartz crystal, as the diffusion coefficient of molecular water in quartz is itself very small.

From the above we have some idea about the parameters for power law creep in the set of experiments from Jaoul et al. (1984) and Jaoul (1984), some constraints from experiments by Kirby and McCormick (1979) on glide in quartz with addition indications from semi-conducting silicon and a selection of available information on silicon and oxygen diffusion in quartz. For a more complete panorama of the parameters for power law creep in quartz polycrystals we have compiled Table 2. When studying Table 2 we realised there was considerable dispersion of the parameters due to the different experimental protocols and specimens. To make more sound comparisons we divided the data into two groups, firstly the data acquired in the laboratory of Jan Tullis at Brown University under her direction, knowing that the protocols are at least similar, and that substantial improvements have been made over the years. A second group with a higher resolution in stress was formed by Gleason and Tullis (1995) using their molten salt assembly at 1.5 GPa, and the experiments done in the Paterson gas apparatus with an internal load cell at 0.3 GPa. The plots of the power law parameters (A, Q and n) of these two groups are shown in Fig. 10. From these plots one might expect to find a correlation between n and A as previously shown for the Dorn equation by Stocker and Ashby (1973) for various materials. The upper part of Fig. 10 show that the data from Brown University at 1.5 GPa show correlations in all 3 plots, with one of the Gleason and Tullis (1995) points not aligning in each plot (importantly not always the same experiment, no melt or melt present). Plots of the high-resolution studies show that only the plot Q versus A gives a good correlation. Several studies have suggested that the constant A should be supplemented by a term  $f(\text{H}_2\text{O})^p$  to represent the fugacity of water (Paterson, 1989; Kohlstedt

et al.1995; Post et al.1996; Hirth et al.,2001; Rutter and Brodie,2004), which at high pressure should be approximately equal to pressure times the fugacity coefficient of water (Hobbs, 1984). Farver and Yund (1991), as well as McConnell (1995), have shown that oxygen diffusion is dependant on water fugacity. Post et al.1996 suggested that the exponent P should be 2, where as Rutter and Brodie (2004) preferred a value of 1, following the analysis of Hirth et al. (2000). Fig. 10, the high-resolution data for A, including the value for Rutter and Brodie is the simple the least-squares fit for A, with no evaluation of a term  $f(\text{H}_2\text{O})^P$  being undertaken. The value of A given by Rutter and Brodie (2004) is  $\log A = -2.45$  (or  $A = 3.5 \times 10^{-3}$ ) when fugacity is not taken into account (used in Fig. 10), where as when A and  $f(\text{H}_2\text{O})$  are use A is reduced to  $\log A = -4.93$  (or  $A = 1.2 \times 10^{-5}$ ); if a similar approach was applied to all the data in figure 10 the fugacity correction would change all A to lower values depending on the value of  $\text{H}_2\text{O}$  fugacity in each experiment. If no other factors contributed to the value of A apart from water fugacity in figure 10, then higher values of A would indicate higher fugacities of water and this would only be true if there is an equilibrium between fugacity and water content of the samples during the experiment. The water fugacity in Rutter and Brodie's experiments was assumed to be the same as the confining pressure of 300 MPa for samples saturated with water, this is likely to be the case for all the experiments done in the Paterson gas rig (i.e. Paterson and Luan, 1990; Luan and Paterson, 1992; and Mainprice and Paterson, 2005). Hirth et al.(2001) estimated that water fugacity in Gleason and Tullis (2005) experiments was 2500 MPa assuming the samples were undersaturated and that the fugacity exponent is one. The A values corrected for these water fugacities do not radically change the correlation between Q and A (figure10) for  $P=1$ . Comparison with Fig. 9 of Q versus wt%  $\text{H}_2\text{O}$  would also suggest a correlation with water content. Intriguingly the plot of Q versus A shows a strong correlation, but the highest pressure studies (Gleason and Tullis, 1995 at 1.5 GPa) do not have the highest value of A. It is possible that the variation of Q with A represents a dependence of Q on water content, in a similar manner to doping for dislocation velocity rather than fugacity. If the doping effect on glide was operating, then both A and Q should decrease with doping concentration, this cannot be established from the current data set. There is also a tendency for the higher resolution studies to a stress exponent between 3 and 4, with exception of silica gel samples. A stress exponent that is significantly higher than 2 tends to suggest that climb is an important component of the deformation mechanism, possibly rate controlling, as glide alone would produce a stress exponent of 2.5 according to Kirby and McCormick, although there may be a contribution of climb to their data. The samples with recognised melt present tend to have low A values in the high resolution data; this is not necessary true in the other data set where all the water-added samples probably have melt present. Melt may possibly also present in some of the 'as-received' samples at higher temperatures.

The range of activation energies for all of table 1 and 2 is quite small with values between about 100 to 250  $\text{kJ mole}^{-1}$ , which cover the range for glide and oxygen diffusion in quartz. Extensive first principles atomic modelling of the hydrogarnet defect with 4 hydrogens at a silicon site  $(4\text{H})_{\text{Si}}$  have shown that this defect has formation energy of 98  $\text{kJ mole}^{-1}$  about half the energy of formation of the Griggs defect (194  $\text{kJ mole}^{-1}$ ) or interstitial water (184  $\text{kJ mole}^{-1}$ ) (Rosa et al.2005; de Leeuw, 2001; McConnell et al.1995; Lin et al.1994; Purton et al.,1992). The activation energy for the diffusion of  $(4\text{H})_{\text{Si}}$  has been estimated to be about 98  $\text{kJ mole}^{-1}$  by Cordier and Doukhan (1989,1991) remarkably closed to the calculated formation energy of Rosa et al.(2005). If the diffusion of hydrogarnet defect is rate controlling for glide or climb, then the activation energy is composed of a 98  $\text{kJ mole}^{-1}$  formation energy plus another contribution of about 37  $\text{kJ mole}^{-1}$  if we accept the synthesis between laboratory and natural deformation made by Hirth et al. (2001) with an activation energy of 135  $\text{kJ mole}^{-1}$ , which would be among the lower values in Table 2. A creep activation energy composed of

formation energy and diffusion activation energy for  $(4H)_{Si}$  would be  $196 \text{ kJ mole}^{-1}$ , still in the range of reported values in table 2. Further constraints on hydrolytic mechanisms will probably come from a better determination of dependence of strain rate on water fugacity or water content. For example current data constrain the fugacity exponent  $P$  to be between 1 and 2, the value of  $P$  greatly reduces the choice of possible point defect models proposed by Hobbs (1984), including models with  $(4H)_{Si}$ . The current range of data on sodium doping is too limited to draw conclusions; the microstructure has been shown here to be rather unique with a very high homogeneous density of dislocations, but the stresses were also very high. The activation energies are higher than other samples measured by Jaoul et al. (1984), but not exceptionally high when compared to the larger data set in table 2. To further understand the mechanism of sodium doping, new experiments are required at lower strains and stresses. It is also clear the further systematic post-mortem analysis of all samples is required to determine water content of each sample; without this, we cannot unravel the macroscopic signal given by the power law constants. Further effort for high resolution stress measurements is also needed at high pressures, the dispersion of the current data set clearly shows that assembly design has significant impact on rheological results in solid medium machines. Unlike other silicates, for example olivine that have intrinsically electrically active defects associated with the valence state of iron (e.g. ferric iron and vacancies at M-sites), that are distributed throughout, quartz requires extrinsic defects that have been introduced by rapid growth, grain boundary sweeping, fractures or diffusion. The effective scale to obtain equilibrium is the given by  $(Dt)^{1/2}$ , which is small even for oxygen (about  $0.2 \mu\text{m}$  at  $1000 \text{ K}$ ) in hydrothermal conditions (e.g. Paterson, 1989), this explains why further progress will probably be made using synthetic fine grained quartz aggregates, rather than single crystals of dimensions that cannot possibly reach thermodynamic equilibrium with their surrounding environment on a laboratory time scale. Alternatively, the use of micron size single crystals would be a more elegant approach for future research (cf Uchic et al., 2004). It is now clear that hydrolytic weakening is not a case of a local effect controlled by diffusion, as opposed to non-local electronic effect controlled by chemical environment, but an equilibrium situation with statistically homogeneously distributed defects versus a non-equilibrium situation, as often portrayed by synthetic quartz crystals super-saturated with respect to water. The presence of dislocation multiplication at bubbles (or precipitates) and association of bubbles with dislocation lines in quartz does not necessarily imply the weakening mechanism is a local phenomenon. The presence of bubbles shows that quartz is often out of equilibrium with respect to the concentration of “water”, and the presence of such mechanical heterogeneities in a crystal structure would result in similar dislocation structures in any material.

## 6. Conclusions

TEM study of Heavitree quartzite deformed at high temperatures and a pressure of  $1.5 \text{ GPa}$  with three different preparations; water added, vacuum dried, and sodium doped show a wide range of dislocation microstructure. The vacuum dried sample shows strong evidence that dislocation glide is difficult, with a high Peierls stress as shown by areas of very low and very high dislocation density and the crystallographic control of dislocation line direction. Dislocation multiplication takes place by cross-slip mechanisms, which do not require diffusion-aided climb. In contrast much lower and more homogeneous dislocation densities are present in the water added sample with abundant evidence for climb including; sub-grain walls, dislocation cells, dislocation junctions and dislocation debris in the form of small loops. Both  $1/3\langle a \rangle$  and  $[c]$  dislocations have been identified in both samples, but  $1/3\langle a \rangle$  appear to be more frequent. The observations of the sodium-doped samples are more difficult to analyse because of the uniformly high dislocation density. In any case, the presence of a high density

of tangled dislocation is evidence for the easy nucleation of dislocations, with strong interactions causing the tangling, which implies climb was not active. The high dislocation densities do not allow us to see if there is crystallographic control of the line directions at these strain levels.

The contributions of dislocation glide velocity, based on the semiconductor literature, and climb enabled by diffusion are reviewed. The activation energy for creep in Heavitree quartzite decreases from 185 kJ/mole in the vacuum dried sample to 151 kJ/mole in 0.39 Wt% H<sub>2</sub>O water added sample. Using previously published data for power creep parameters ( $A$ ,  $Q$ ,  $n$ ) from experiments with high-stress resolution, we see a similar correlation between the pre-factor  $A$  and activation energy  $Q$ . In semi-conductors, doping level also affects the pre-factor and the activation energy for glide. The pre-factor  $A$  also includes some information on the water fugacity if we follow previous suggestions in the literature. Making a correction to  $A$  for the contribution of water fugacity does not remove this correlation, so we suggest it might in part be due to water concentration in the samples, as the hydrogarnet defect which has a lower formation energy than the Griggs defect and interstitial water.

### Acknowledgements

DM thanks Sir Peter Hirsch for access to the high voltage transmission microscopy facility at Oxford University during the course of this study. DM also thanks Pirous Pirous for helpful discussions about dislocation velocities in semi-conductors during his stay at Oxford. DM thanks both reviews and editor David Kohlstedt for their constructive comments, and especially Andreas Kronenberg for his many corrections. Any flaws remaining in this manuscript are the fault of the first author.

### References

- Baluffi, R.W., Seidman, D.N. 1972. Void formation in quenched or irradiated materials. In: *Radiation-induced Voids in Metals* (Ed. By J.W. Corbett and L.C. Ianniello) p.563. U.S.A.E.C., Oak Ridge.
- Blacic J.D., Christie J.M., 1984. Plasticity and hydrolytic weakening of quartz single crystals. *J. Geophys. Res.* 89, 4223-4239.
- Brady, J.B., 1995. Diffusion Data for Silicate Minerals, Glasses, and Liquids. In *Mineral Physics and Crystallography – A handbook of physical constants*, AGU Reference Shelf 2, 269-290.
- Charles, R.J., Hillig, W.B., 1962. The kinetics of glass failure by stress corrosion. In *Symposium sur la Resistance Mechanique du Verre*, Charleroi, Belgium, p.511.
- Cordier, P., Doukhan, J.C., 1989. Water in quartz; solubility and influence on ductility - *European Journal of Mineralogy*, 1, 221-237.
- Cordier P., Doukhan J.C., 1991. Water speciation in quartz—a near-infrared study. *Amer Mineral* 76:361–369
- Cordier, P., Weil, J.A., Howarth, D.F., Doukhan, J.C., 1994. Influence of the (4H)Si defect on dislocation motion in crystalline quartz - *European Journal of Mineralogy*, 6, 17-22.

- Dennis, P. F., 1984. Oxygen selfdiffusion in quartz under hydrothermal conditions, *J. Geophys. Res.*, 89, 4047-4057.
- Giletti, B.,J., Yund, R.A., 1984. Oxygen diffusion in quartz, *J. Geophys. Res.*, 89, 4039-4046.
- Farver, J.R., Yund, R. A., 1991. Oxygen fugacity in quartz: dependence on temperature and water fugacity. *Chem. Geol.* 90, 55-70.
- Frischat, G., 1970. Sodium diffusion in natural quartz crystals. *J. Am. Ceram. Soc.*, 53, 357.
- Gleason, G.C., Tullis, J., 1995. A flow law for dislocation creep of quartz aggregates determined with the molten salt cell. *Tectonophysics* 247,1–23.
- Griggs, D.T., 1967. Hydrolytic weakening in quartz and other silicates. *Geophys. J.R. astr. Soc.*,14, 19-31.
- Griggs D.T., Blacic, J.D., 1965. Quartz: Anomalous weakness of synthetic crystals. *Science* 147, p. 292 – 295.
- Haasen, P., 1979. Kink formation and migration as dependent on the Fermi level. *J. du Phys. Orsay Fr* , 40, 111-116.
- Hirsch, P.B., 1979. A mechanism for the effect of doping on dislocation mobility. *J. du Phys. Orsay Fr* , 40, 117-121.
- Hirsch, P.B., 1981. Plastic deformation and electronic mechanisms in semi-conductors and insulators. *J. du Phys. Colloq. C3*, 42, 149-160.
- Hirsch P.B., Humphreys F.J., 1970. *Proc. Roy. Soc.* A318, 45.
- Hirth, G., Teyssier C., Dunlap W.J., 2001. An evaluation of quartzite flow laws based on comparisons between experimentally and naturally deformed rocks. *Int. J. Earth Sciences* 90, 77-87.
- Fitz Gerald, J. D., Boland, J. N., McLaren, A. C., Ord, A., Hobbs, B. E., 1991. Microstructures in water-weakened single crystals of quartz. *J. Geophys. Res.* 96, 2139–2155.
- Hobbs, B.E., 1981. The influence of metamorphic environment upon the deformation of minerals. *Tectonophysics*, 78, 335-383.
- Hobbs, B.E., 1984. Point defect chemistry of minerals under a hydrothermal environment. *J. Geophys. Res.*, 89, 4026-4038.
- Jaoul, O., 1984. Sodium weakening of Heavitree quartzite ; preliminary results. *J. Geophys. Res.*, 89, 4271-4280.
- Jaoul,O. Poumellic, M., Froidveaux, C., Havette, A., 1981. Silicon diffusion in forsterite : a new constraint for understanding mantle deformation, in “Anelasticity in the Earth”, *Geodyn. Ser.*, Vol. 4, edited by F.D. Stacey, M.S. Paterson and A. Nicolas, pp 95-100,AGU, Washington, D.C.,USA.

Jaoul, O., Tullis, J., Kronenberg, A. K., 1984. The effect of varying water contents on the creep behavior of Heavitree quartzite, *Jour. Geophys. Res.*, 89, 4298-4312.

Jaoul, O., Bédjina, F., Élie, F., Abel, F., 1995. Silicon self-diffusion in quartz. *Phys. Rev. Lett.*, 74, 2038-2041.

Johnston, W.G., Gilman, J.J., 1959. Dislocation velocities, dislocation densities and plastic flow of lithium fluoride crystals. *J. Appl. Phys.* 30, 129-135.

Kirby S.H., McCormick, J.W., 1979. Creep of hydrolytically weakened synthetic quartz crystals oriented to promote  $\{2\bar{1}\bar{1}0\}$   $\langle 0001 \rangle$  slip: a brief summary of work to date. *Bull Minéral* 102:124–137

Koch, P.S., Christie, J.M., Ord, A., George, Jr., R.P., 1989. Effect of water on the rheology of experimentally deformed quartzite. *Journal of Geophysical Research* 94, 13975–13996.

Kohlstedt, D.L., Hornack, P., 1981. Effect of oxygen partial pressure on the creep of olivine, in “Anelasticity in the Earth”, *Geodyn. Ser.*, Vol. 4, edited by F.D. Stacey, M.S. Paterson and A. Nicolas, pp 101-107, AGU, Washington, D.C., USA.

Kohlstedt, D.L., Evans, B., Mackwell, S.J., 1995. Strength of the lithosphere: constraints imposed by laboratory experiments. *Journal of Geophysical Research* 100, 17587–17602.

Kronenberg, A. K., Kirby, S. H., Aines, R. D., Rossman, G. R., 1986. Solubility and diffusional uptake of hydrogen in quartz at high water pressures: implications for hydrolytic weakening, *Jour. Geophys. Res.*, 91, 12723-12744.

Kronenberg, A. K., Wolf, G. H., 1990. FTIR determinations of intragranular water content in quartz-bearing rocks: implications for hydrolytic weakening in the laboratory and within the Earth, *Tectonophysics*, 172, 255-271.

de Leeuw, N.H., 2001. Density functional theory calculations of hydrogen-containing defects in forsterite, periclase, and  $\alpha$ -quartz. *J. Phys. Chem.* 105, 9747–9754.

Lin, J.S., Payne, M.C., Heine V., McConnell, J.D., 1994. Ab-initio calculations on  $(\text{OH})_4$  defects in  $\alpha$ -quartz. *Phys. Chem. Mineral.* 21, 150–155.

Luan, F.C., Paterson, M.S., 1992. Preparation and deformation of synthetic aggregates of quartz. *Journal of Geophysical Research* 97, 301–320.

McConnell, J.D.C., 1995. The role of water in oxygen isotope exchange in quartz. *Earth Planet. Sci. Lett.* 136, 97-107.

McConnell, J.D.C., Lin J.S., Heine, V., 1995. The solubility of  $[\text{4H}]\text{Si}$  defects in  $\alpha$ -quartz and their role in the formation of molecular water and related weakening on heating. *Phys. Chem. Mineral.* 22, 357–366.

McLaren, A.C., Cook, R.F., Hyde, S.T., Tobin, R.C., 1983. The mechanisms of the formation and growth of water bubbles and associated dislocation loops in synthetic quartz. *Phys Chem Minerals*, 9, 79-94.

McLaren, A.C., Fitz Gerald, J.D., Gerretsen, J., 1989. Dislocation nucleation and multiplication in synthetic quartz: relevance to water weakening. *Phys. Chem. Mineral.* 16, 465-482

Mainprice, D.H., 1981. The experimental deformation of quartz polycrystals. Ph.D thesis. Australian National University, Canberra, 171pp.

Mainprice D., Paterson M.S., 1984. Experimental studies on the role of water in the plasticity of quartzites. *J. Geophys. Res.*, 89, 4257-4269.

Mainprice D., Paterson M.S., 2005 Experimental deformation of flint in axial compression. In Bruhn, D. and Burlini, L. (eds) High-strain zones : Structures and physical properties, *Geol. Soc. Lond. Special publication*, 245, 251-276.

Morrison-Smith, D.J., Paterson, M.S., Hobbs, B.E., 1976. An electron microscope study of plastic deformation in single crystals of synthetic quartz. *Tectonophysics*, 33, 43-79.

Patel, J.R., Testardi, L.R., Freeland, P.E., 1976. Electronic effects on dislocation velocities in heavily doped silicon. *Physical Review B* 13, 3548-3557.

Paterson, M.S., 1982. The determination of hydroxyl by infrared absorption in quartz, silicate glasses and similar materials. *Bull. Minéral.*, 105, 20-29.

Paterson, M.S., 1989. The interaction of water with quartz and its influence in dislocation flow-an overview. In: Karato, S.I., Toriumi, M. (Eds.), *Rheology of Solids and of the Earth*. Oxford University Press, Oxford, 107-142.

Paterson, M.S., Luan, F.C., 1990. Quartzite rheology under geological conditions. In: Knipe, R.J., Rutter, E.H (Eds.), *Deformation mechanisms, rheology, and tectonics*. Geologic Society of London Special Publication 54, 299-307.

Post, A.D., Tullis, J., Yund, R.A., 1996. Effects of chemical environment on dislocation creep. *Journal of Geophysical Research* 101, 22143-22155.

Post A.D., Tullis, J., 1998. The rate of water penetration in experimentally deformed quartzite: implications for hydrolytic weakening. *Tectonophysics* 295, 117-137.

Purton, J., Jones, R., Heggie, M.I., Oberg, S., Catlow, C.R.A., 1992. LDF Pseudopotential calculations of the  $\alpha$ -quartz structure and hydrogarnet defect. *Phys. Chem. Mineral.* 18, 389-392.

Rovetta, M., Holloway, J.R., Blacic, J.D., 1986. Solubility of hydroxyl in natural quartz annealed in water at 900°C and 1.5 GPa. *Geophys. Res. Lett.* 13, 145-148.

Rosa, A.L., El-Barbary, A.A., Heggie, M.I., Briddon, P.R., 2005. Structural and thermodynamic properties of water related defects in  $\alpha$ -quartz. *Phys. Chem. Minerals* 32,

323-331.

Rutter, E.H., Brodie, K.H., 2004. Experimental intracrystalline plastic flow in hot-pressed synthetic quartzite prepared from Brazilian quartz crystals. *J. Struct. Geology* 26,259-270.

Rybach, L., Laves, F., 1967. Sodium diffusion experiments in quartz crystals. *Geochim. Cosmochim. Acta* 31, 539-546.

Schröter, W., Labusch, R., Haasen, P., 1977. Comment on 'Electronic effects on dislocation velocities in heavily doped silicon' by J.R.Patel, L.R.Testardi, and P.E. Freeland. *Physical Review B* 15, 4121- 4123.

Stocker, R.L., Ashby, M.F. ,1973. On the empirical constants in the Dorn equation. *Scripta Metallurgica* 7, 115-120.

Stipp, M., Tullis, J., Behrens, H., 2006. Effect of water on the dislocation creep microstructure and flow stress of quartz and implications for the recrystallized grain size piezometer. *J. Geophys. Res.*, 111, B04201, doi:10.1029/2005JB003852.

Uchic, M.D., Dimiduk, D.M., Florando, J.N., Nix, W.D., 2004. Sample dimensions influence strength and crystal plasticity. *Science* 305, 986-989.

Wu, C.-K., 1980. Stable silicate glasses containing up to 10 wt% water. *J. Non-crystalline Solids*, 41, 381-398.

Yonenaga, I., 2001. Dislocation behavior in heavily impurity doped Si. *Scripta Materialia* 45, 1267-1272.

## Figure Captions

Fig. 1. Stress – strain rate lines for Heavitree quartzite at a pressure of 1.5 GPa extrapolated to a common temperature of 800°C. Data from Jaoul et al.(1984) and Jaoul (1984).

Fig. 2. Bright field TEM images at 120 kV of water added sample W-300. A – melt pocket with inset diffraction pattern from melt showing amorphous structure. B – Melt showing limited penetration into grain boundary. C- Low angle melt film on grain boundary with locally high dislocation density at contact. D – Melt free grain boundary with stepped structure and fringes.

Fig. 3. Bright field TEM images at 120 kV of water added sample W-300. A- cusped grain boundary of grain containing dislocations associated with bubbles. B- Serrated grain boundary with large voids or bubbles. C – Well-formed dislocation boundaries with variable orientation, note 120° degree dislocation triple junctions. D – Low-density dislocation network, small dislocation loop debris and long straight dislocation parallel to c-axis.

Fig. 4. Bright field TEM images of water added sample W-300. A – 1000 kV image of dislocation cells. B – 120 kV image of sub-grain all close to  $(2\bar{1}\bar{1}0)$  plane with  $W=0$ . C- 120 kV image  $\langle a \rangle$  dislocations out of contrast,  $W>0$ . C - 120 kV image  $[c]$  dislocations out of contrast,  $W>0$ .  $W$  is deviation from exact Bragg diffracting condition.

Fig. 5. Bright field images at 120 kV of water added sample W-300. Dislocation analysis using 4 diffracting vectors and two beam orientation using dislocation image simulation matching. See text for details.

Fig. 6. Bright field TEM images of vacuum dried sample W-302 at 1000 kV. A – shear bands in (0001) plane with dislocation nucleation at Frank-Read (FR) source. B – Parallel shears bands in (0001) plane with moderate dislocation density in between. C- Relatively wide (0001) shear bands in low contrast.

Fig. 7. TEM bright (BF) and dark field (DF) images. A- BF 120 kV water added sample, detail of bubbles. B – DF 120 kV water added sample, detail of bubbles along dislocation parallel to c-axis. C DF 1000 kV vacuum dried sample, dislocation multiplication at small hard inclusions. D – BF 1000 kV sodium doped sample (W-303) with uniform high dislocation density of tangled dislocations. Note dislocation (D) in grain boundary interface.

Fig. 8. Activation energy for creep versus water content in Heavitree quartzite. Note the water content in wt.% is only a relative scale.

Fig. 9. Activation energy for dislocation glide versus dopant concentration in single crystal silicon at ambient pressure and 600°C (Data from Patel et al.1976).

Fig. 10. Power law creep parameters  $A$ ,  $Q$  and  $n$  for quartz aggregates. The open circles in the High resolution flow laws plot of activation energy versus  $A$  constant are corrections to  $A$  assuming that water fugacity dependence to the power of one. See text for discussion.

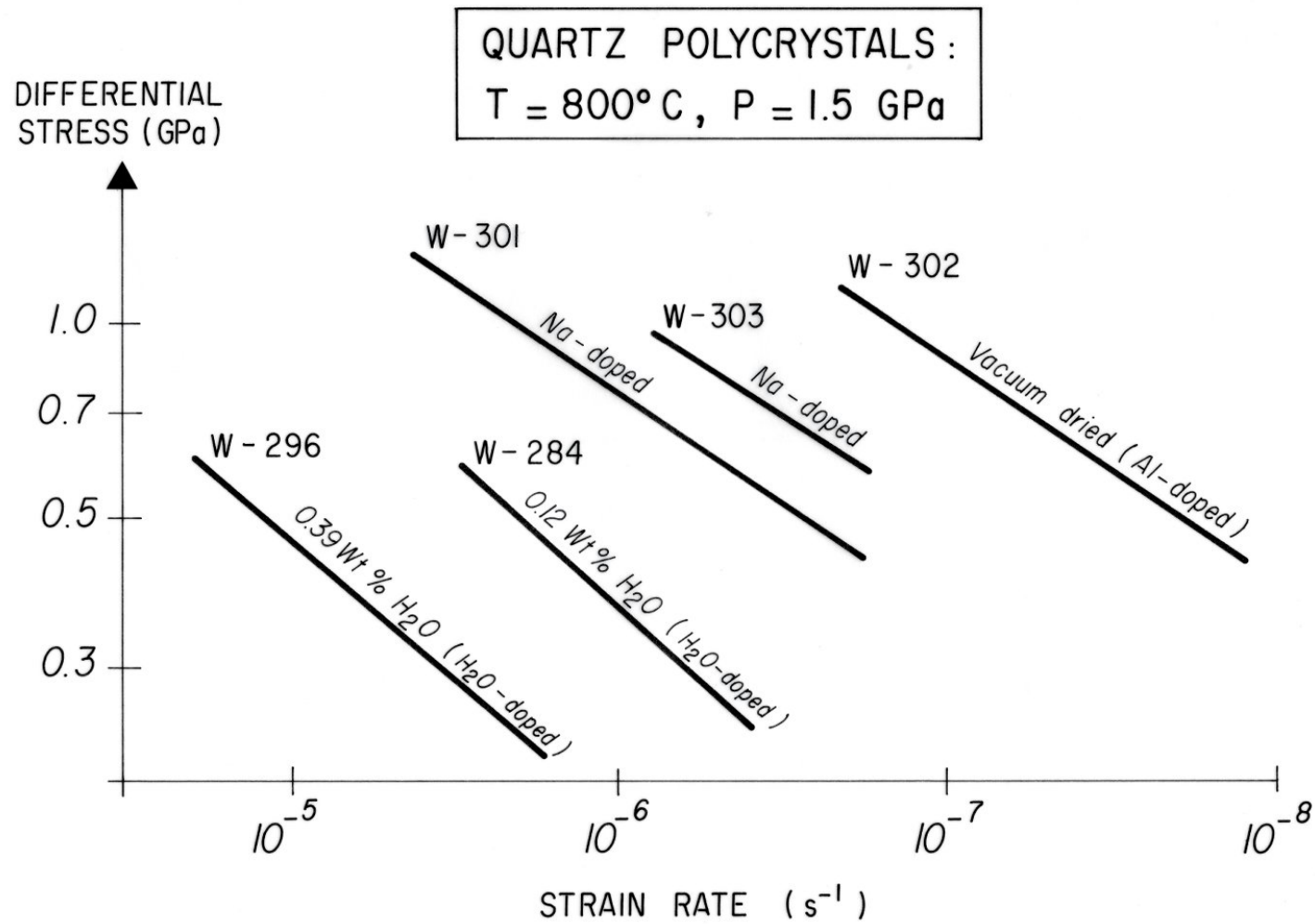


Fig. 1. Stress – strain rate lines for Heavitree quartzite at a pressure of 1.5 GPa extrapolated to a common temperature of 800°C. Data from Jaoul et al.(1984) and Jaoul (1984).

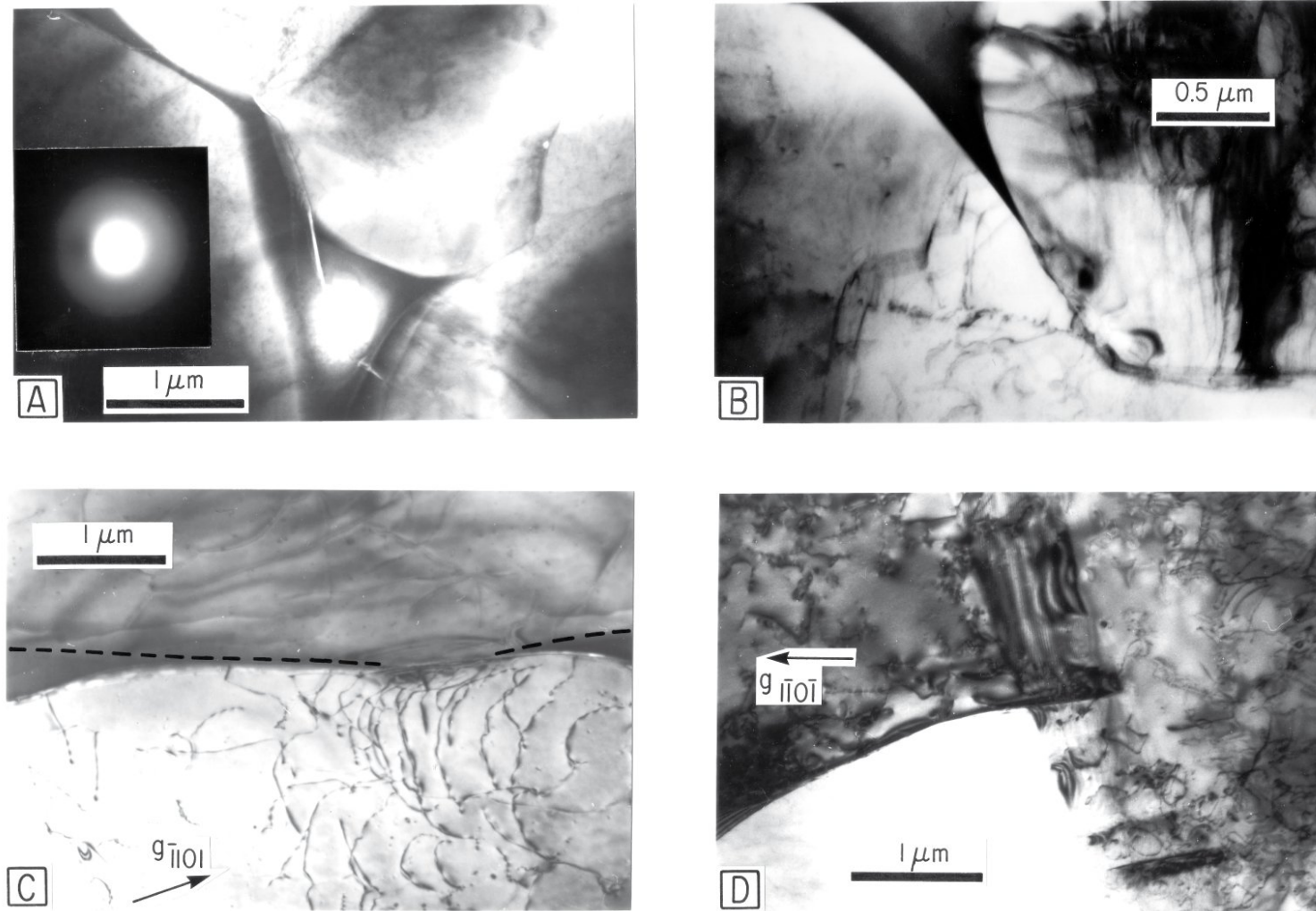


Fig. 2. Bright field TEM images at 120 kV of water added sample W-300. A – melt pocket with inset diffraction pattern from melt showing amorphous structure. B – Melt showing limited penetration into grain boundary. C- Low angle melt film on grain boundary with locally high dislocation density at contact. D – Melt free grain boundary with stepped structure and fringes.

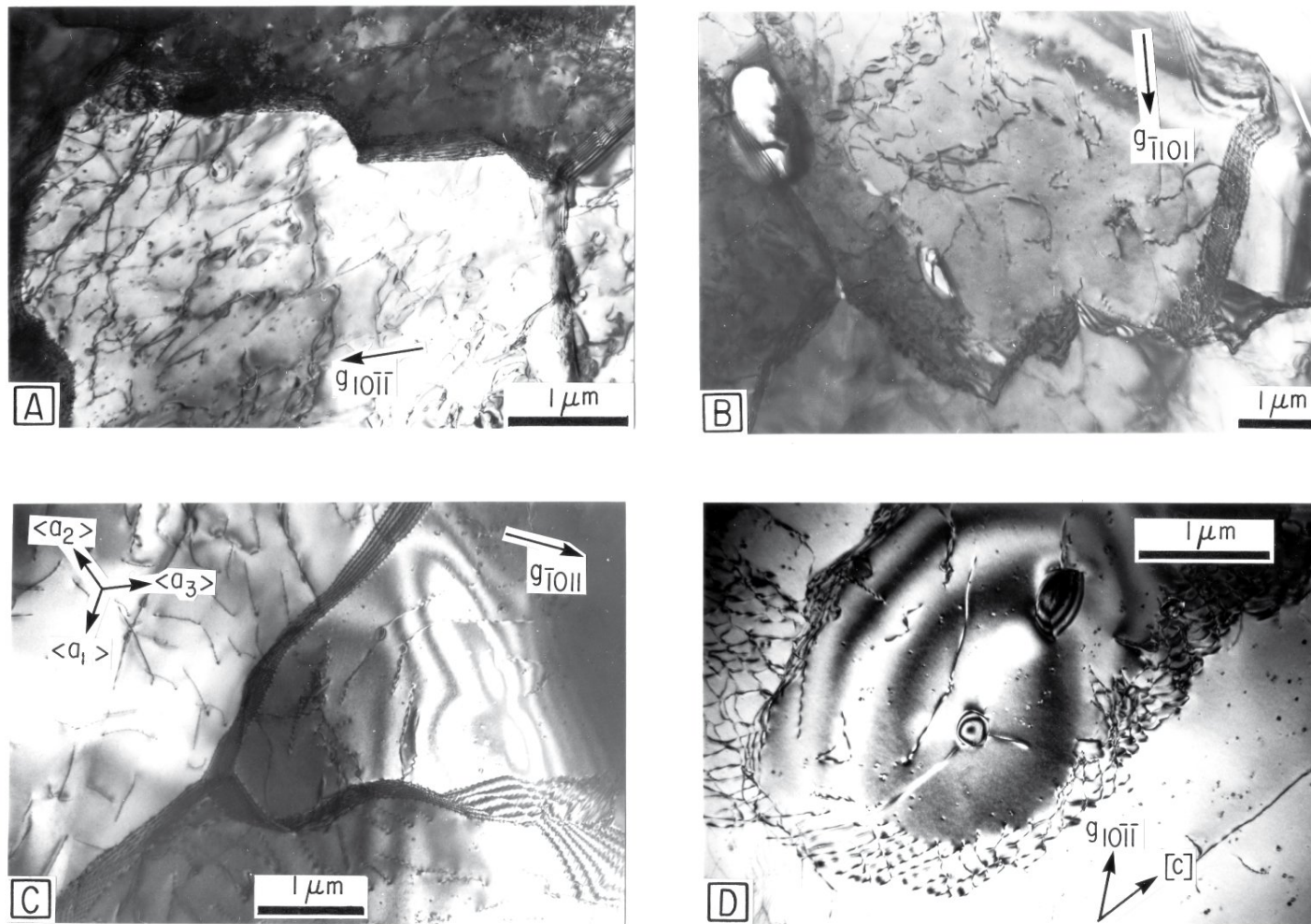


Fig. 3. Bright field TEM images at 120 kV of water added sample W-300. A- cusped grain boundary of grain containing dislocations associated with bubbles. B- Serrated grain boundary with large voids or bubbles. C – Well-formed dislocation boundaries with variable orientation, note 120° degree dislocation triple junctions. D – Low-density dislocation network, small dislocation loop debris and long straight dislocation parallel to c-axis.

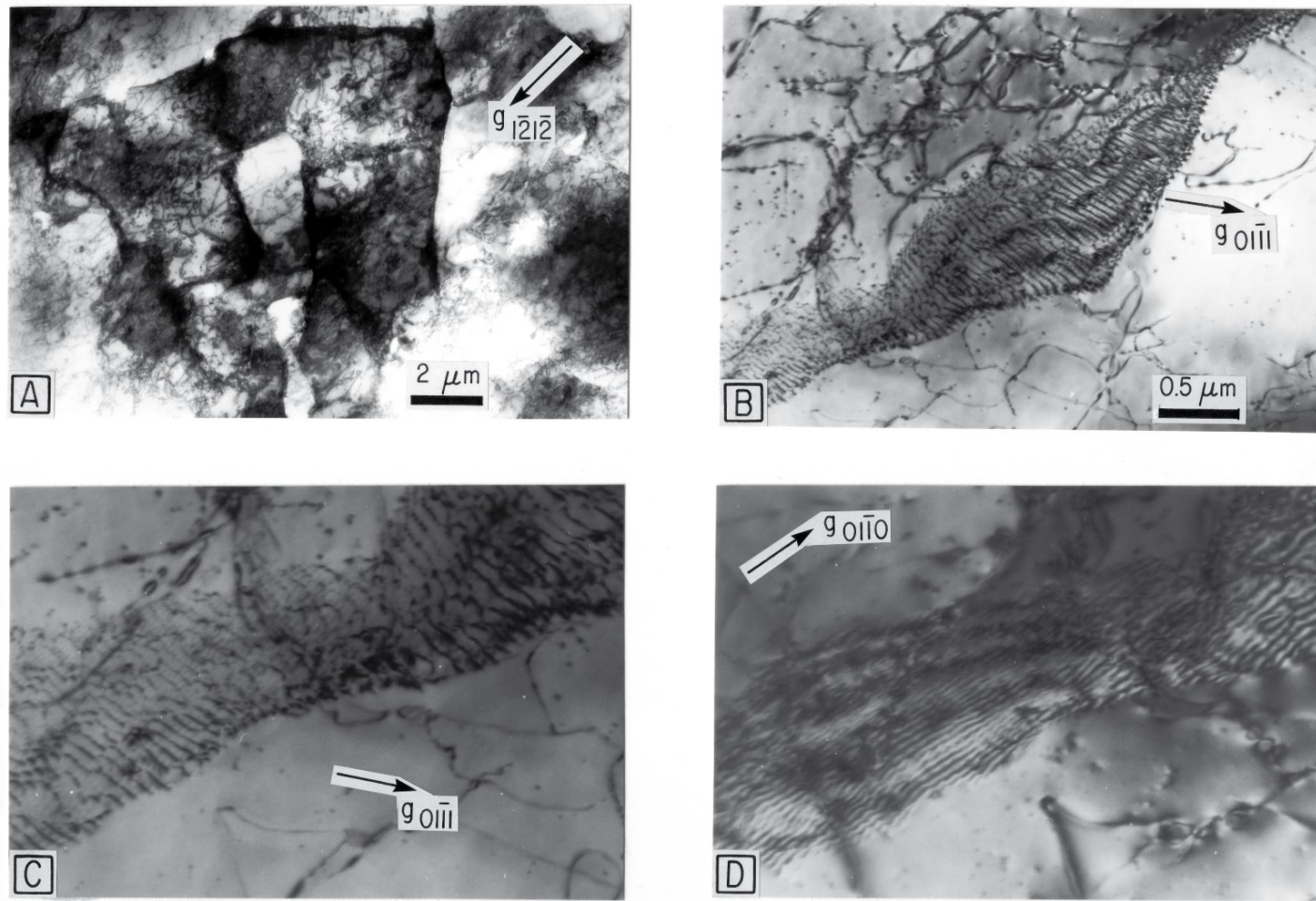


Fig. 4. Bright field TEM images of water added sample W-300. A – 1000 kV image of dislocation cells. B – 120 kV image of sub-grain all close to  $(2\bar{1}\bar{1}0)$  plane with  $W=0$ . C- 120 kV image  $\langle a \rangle$  dislocations out of contrast,  $W>0$ . C - 120 kV image  $\langle c \rangle$  dislocations out of contrast,  $W>0$ .  $W$  is deviation from exact Bragg diffracting condition.

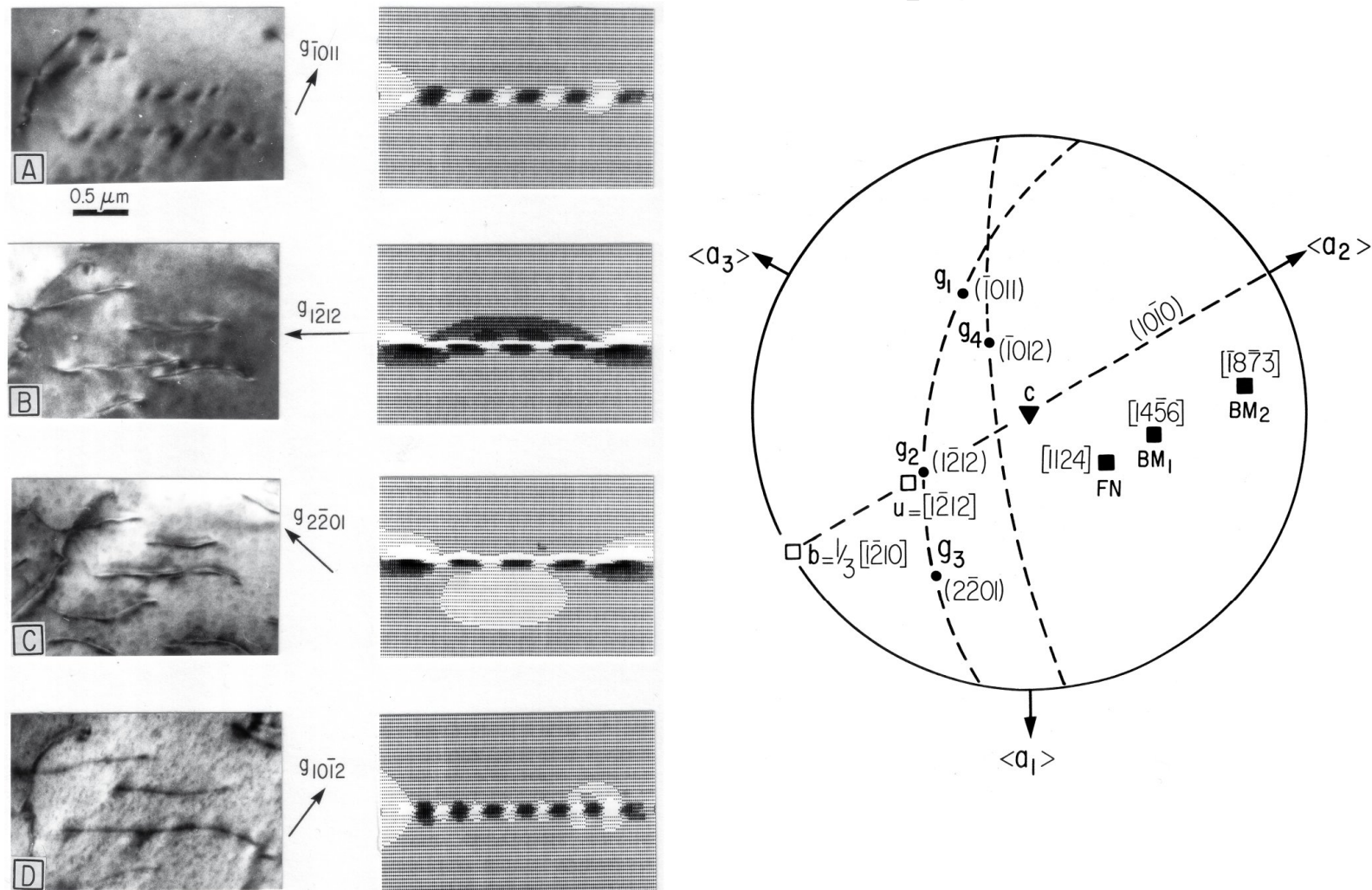


Fig. 5. Bright field images at 120 kV of water added sample W-300. Dislocation analysis using 4 diffracting vectors and two beam orientation using dislocation image simulation matching. See text for details.

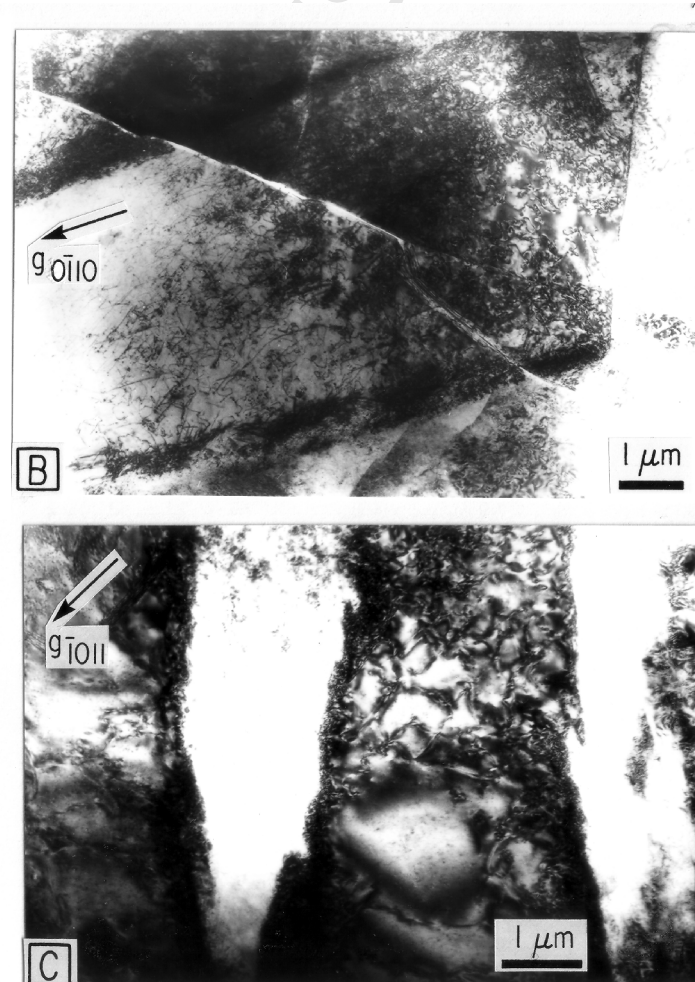


Fig. 6. Bright field TEM images of vacuum dried sample W-302 at 1000 kV. A – shear bands in (0001) plane with dislocation nucleation at Frank-Read (FR) source. B – Parallel shears bands in (0001) plane with moderate dislocation density in between. C- Relatively wide (0001) shear bands in low contrast. D- High magnification view of a shear band showing a dislocation core labeled 'd'.

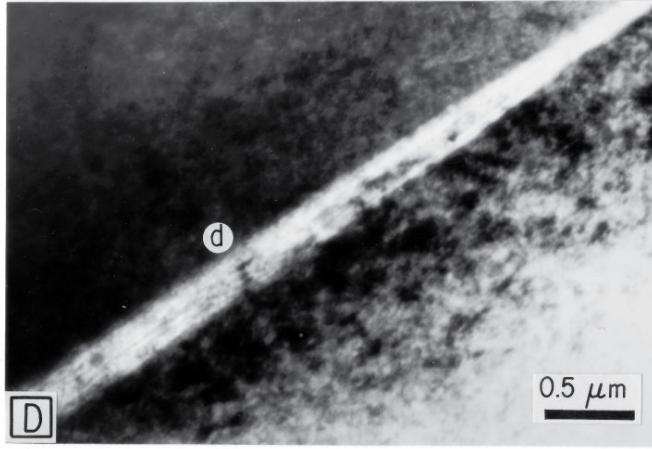
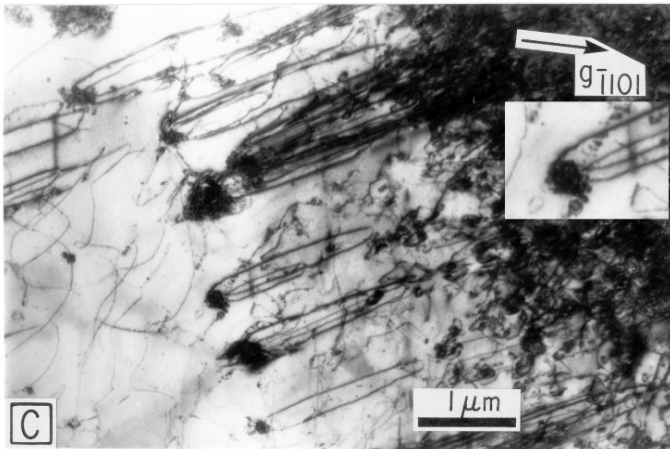
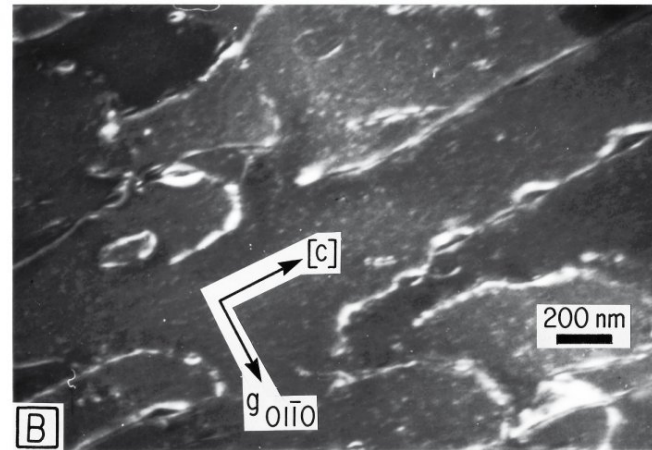
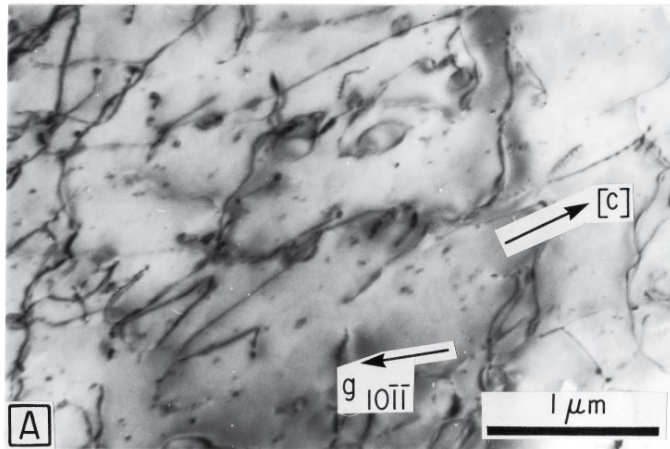


Fig. 7. TEM bright (BF) and dark field (DF) images. A- BF 120 kV water added sample, detail of bubbles. B – DF 120 kV water added sample, detail of bubbles along dislocation parallel to c-axis. C DF 1000 kV vacuum dried sample, dislocation multiplication at small hard inclusions. D – BF 1000 kV sodium doped sample (W-303) with uniform high dislocation density of tangled dislocations. Note dislocation (D) in grain boundary interface.

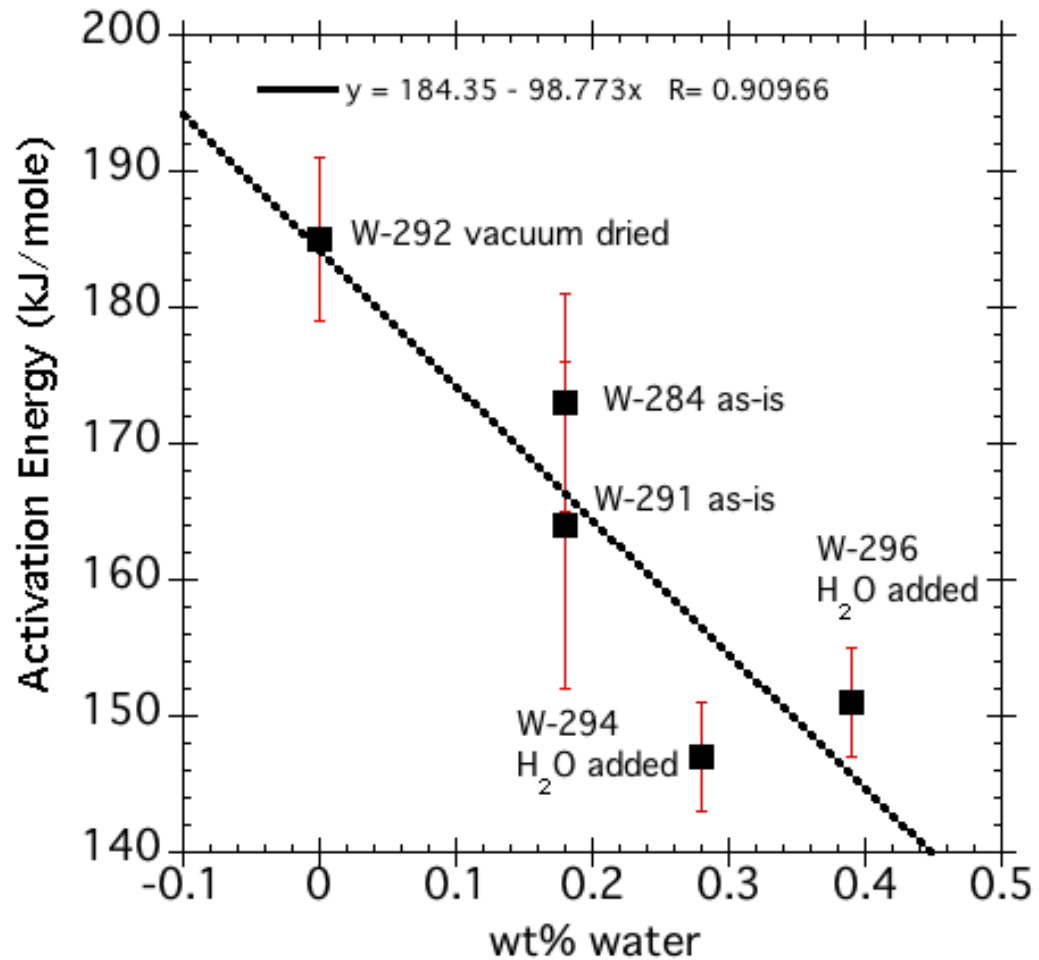


Fig. 8. Activation energy for creep versus water content in Heavitree quartzite. Note the water content in wt.% is only a relative scale.

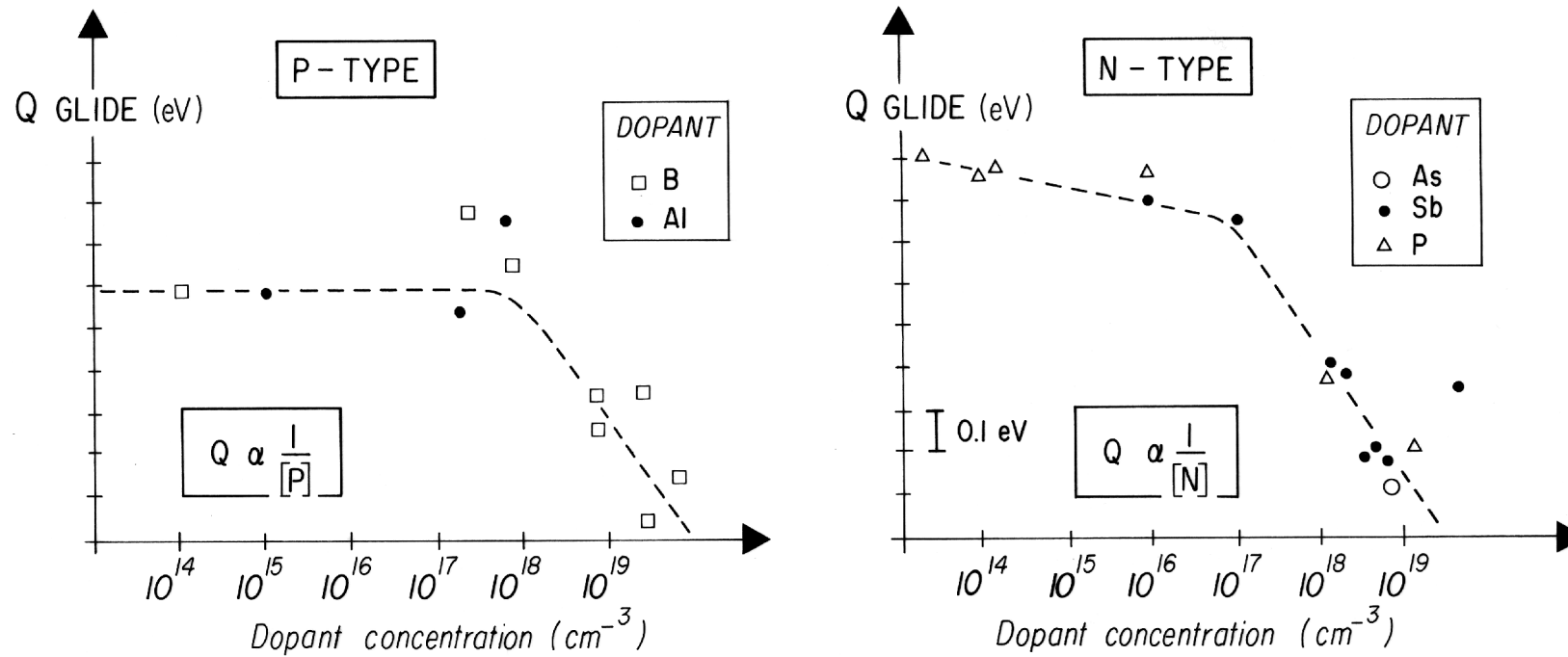
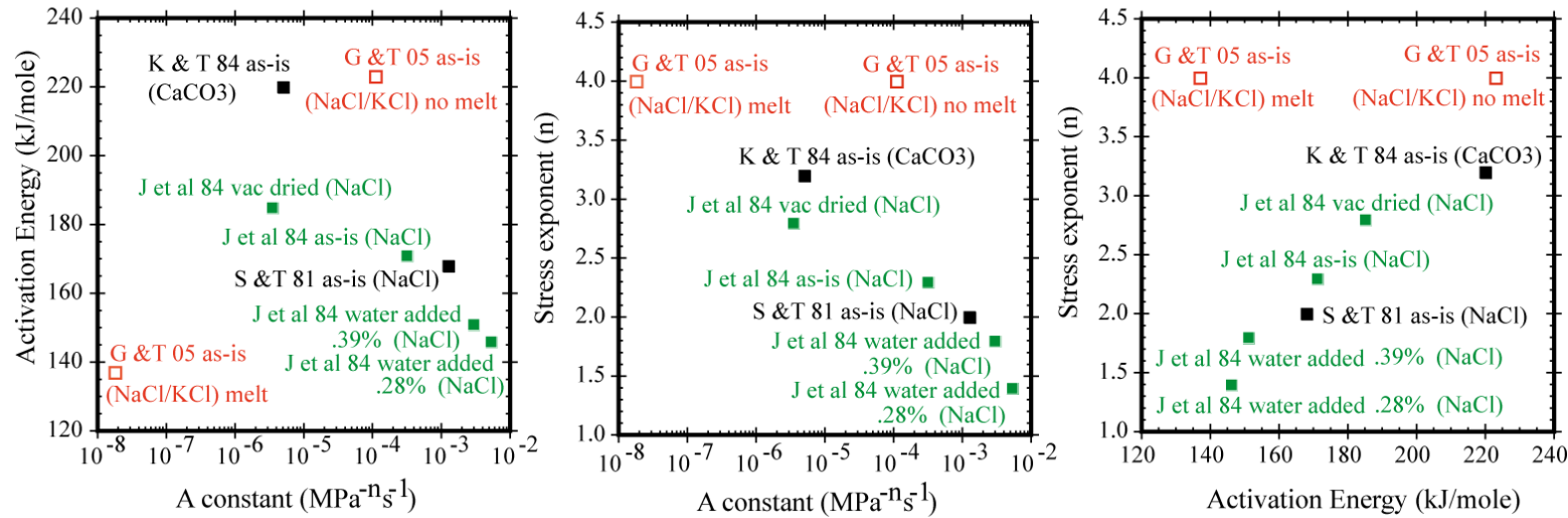


Fig. 9. Activation energy for dislocation glide versus dopant concentration in single crystal silicon at ambient pressure and 600°C (Data from Patel et al.1976).

## Flow laws at 1.5 GPa from the Lab of Jan Tullis



## High resolution flow laws

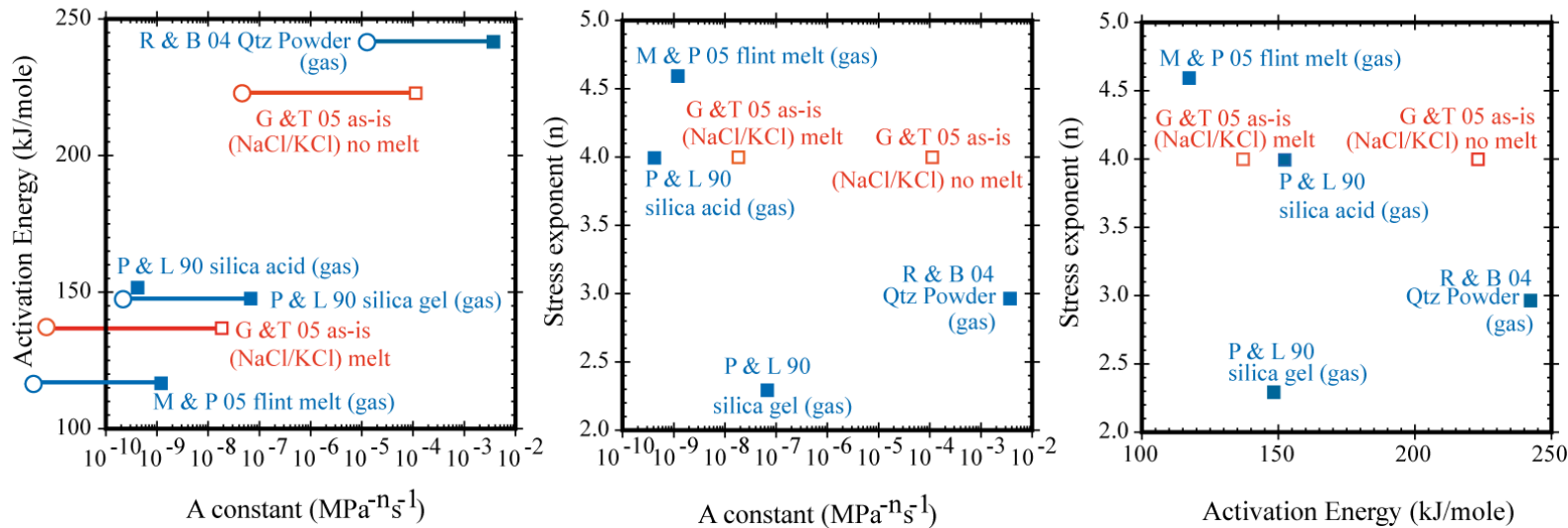


Fig. 10. Power law creep parameters A, Q and n for quartz aggregates. The open circles in the High resolution flow laws plot of activation energy versus A constant are corrections to A assuming that water fugacity dependence to the power of one. See text for discussion.

Accepted Manuscript

Table 1 Experimental Data

| Sample      | Temperature Range °C | Strain (%) | Stress Exponent (n) | Activation Energy (kJ/mole) | Remarks                                       |
|-------------|----------------------|------------|---------------------|-----------------------------|---|
| W-292       | 1050-700             | 27.0       | $2.8 \pm 0.2$       | $185 \pm 6$                 | Vacuum dried at 685°C for 4 days              |
| W-302 (TEM) | 890-800              | 11.0       | $3.3 \pm 0.4$       |                             | Vacuum dried at 1010°C for 5.5 hours          |
| W-301       | 900-800              | 12.5       | $3.4 \pm 0.5$       | $205 \pm 35$                | Na-doped (vacuum dried plus sodium diffusion) |
| W-303 (TEM) | 890-800              | 16.7       | $3.1 \pm 0.2$       | $245 \pm 45$                | Na-doped (vacuum dried plus sodium diffusion) |
| W-300 (TEM) | 900                  | 18.0       |                     |                             | 0.42 wt% water (water-added)                  |
| W-296       | 800                  | 21.0       | $1.8 \pm 0.2$       | 151                         | 0.39 wt% water (water-added)                  |
| W-294       | 1000-700             | 30.0       | $1.4 \pm 0.1$       | $147 \pm 4$                 | 0.28 wt% water (water-added)                  |
| W-284       | 900-650              | 21.0       | $2.3 \pm 0.1$       | $173 \pm 8$                 | 0.18 wt% water (as-is)                        |
| W-291       | 1050-850             | 27.0       | $2.4 \pm 0.4$       | $164 \pm 12$                | 0.18 wt% water (as-is)                        |

Table 2: Power law constants for quartz polycrystals

| Reference                 | A (MPa <sup>-n</sup> s <sup>-1</sup> ) | n   | Q (kJ mole <sup>-1</sup> ) | Pressure (GPa) | Pressure Medium   | Remarks                             |
|---------------------------|--|-----|----------------------------|----------------|-------------------|-------------------------------------|
| Heard & Carter 1968       | $7.90 \times 10^{-11}$                 | 5.7 | 244                        | 0.8            | gas               | Simpson as-is                       |
| Parrish et al. 1976       | $3.98 \times 10^{-02}$                 | 2.6 | 231                        | 1.0            | Talc              | Canyon Greek water from talc        |
| Shelton & Tullis 1981     | $1.26 \times 10^{-03}$                 | 2.0 | 168                        | 1.5            | NaCl              | Heavitree as-is                     |
| Kronenberg & Tullis 1984  | $5.00 \times 10^{-06}$                 | 3.2 | 220                        | 1.5            | CaCO <sub>3</sub> | Heavitree as-is                     |
| Jaoul et al. 1984         | $3.10 \times 10^{-04}$                 | 2.3 | 171                        | 1.5            | NaCl              | Heavitree as-is                     |
| Jaoul et al. 1984         | $3.44 \times 10^{-06}$                 | 2.8 | 185                        | 1.5            | NaCl              | Heavitree vacuum dried              |
| Jaoul et al. 1984         | $5.26 \times 10^{-03}$                 | 1.4 | 146                        | 1.5            | NaCl              | Heavitree water added .28wt%        |
| Jaoul et al. 1984         | $2.91 \times 10^{-03}$                 | 1.8 | 151                        | 1.5            | NaCl              | Heavitree water added .39wt%        |
| Koch et al. 1989          | $1.16 \times 10^{-07}$                 | 2.7 | 134                        | 1.5            | Cu                | Simpson as-is                       |
| Koch et al. 1989          | $5.05 \times 10^{-06}$                 | 2.6 | 145                        | 1.5            | Cu                | Simpson water added                 |
| Gleason & Tullis 1995     | $1.10 \times 10^{-04}$                 | 4.0 | 223                        | 1.5            | NaCl/KCl          | Black Hills as-is no melt           |
| Gleason & Tullis 1995     | $1.80 \times 10^{-08}$                 | 4.0 | 137                        | 1.5            | NaCl/KCl          | Black Hills as-is melt present      |
| Paterson & Luan 1990      | $6.50 \times 10^{-08}$                 | 2.3 | 148                        | 0.3            | gas               | Silica gel                          |
| Paterson & Luan 1990      | $4.00 \times 10^{-10}$                 | 4.0 | 152                        | 0.3            | gas               | Silica acid                         |
| Rutter & Brodie 2004      | $3.54 \times 10^{-03}$                 | 3.0 | 242                        | 0.3            | gas               | Brazilian quartz powder water added |
| Mainprice & Paterson 2005 | $1.15 \times 10^{-09}$                 | 4.6 | 117                        | 0.3            | gas               | Flint as-is melt present            |